nature biotechnology

Article

https://doi.org/10.1038/s41587-023-02060-8

IL-10-expressing CAR T cells resist dysfunction and mediate durable clearance of solid tumors and metastases

Received: 1 April 2022

Accepted: 8 November 2023

Published online: 02 January 2024

Check for updates

Yang Zhao[1,2,8], Jiangqing Chen[3,8], Massimo Andreatta[4,5], Bing Feng[1,2], Yu-Qing Xie[1], Mathias Wenes[4], Yi Wang[1,2], Min Gao[1], Xiaomeng Hu[1], Pedro Romero[4], Santiago Carmona[4,5], Jie Sun[3], Yugang Guo[1,2,6,7] & Li Tang[1,2]

The success of chimeric antigen receptor (CAR) T cell therapy in treating several hematopoietic malignancies has been difficult to replicate in solid tumors, in part because of T cell exhaustion and eventually dysfunction. To counter T cell dysfunction in the tumor microenvironment, we metabolically armored CAR T cells by engineering them to secrete interleukin-10 (IL-10). We show that IL-10 CAR T cells preserve intact mitochondrial structure and function in the tumor microenvironment and increase oxidative phosphorylation in a mitochondrial pyruvate carrier-dependent manner. IL-10 secretion promoted proliferation and effector function of CAR T cells, leading to complete regression of established solid tumors and metastatic cancers across several cancer types in syngeneic and xenograft mouse models, including colon cancer, breast cancer, melanoma and pancreatic cancer. IL-10 CAR T cells also induced stem cell-like memory responses in lymphoid organs that imparted durable protection against tumor rechallenge. Our results establish a generalizable approach to counter CAR T cell dysfunction through metabolic armoring, leading to solid tumor eradication and long-lasting immune protection.

Chimeric antigen receptor (CAR) T cell therapy has achieved remarkable clinical success in treating B cell malignancies. However, CAR T cells have so far shown limited efficacy against solid tumors, and long-term disease control remains rare. One of the major factors that hinders the efficacy of CAR T cell therapy is T cell dysfunction in tumors due to T cell exhaustion[1]. Exhausted T cells are characterized as a distinct population with complete or partial loss of proliferative capacity and effector function, upregulation of multiple immune inhibitory receptors and transcriptional and epigenetic alterations[2–5]. Metabolic fitness is essential to sustain T cell survival and function. Emerging evidence suggests that metabolic alteration and deficiency of intratumoral T cells drive T cell exhaustion[6–8]. Mitochondrial dysfunction imposed by mitochondrial depolarization and oxidative stress was shown to reinforce phenotypic and epigenetic exhaustion programs

[1]Institute of Bioengineering, École Polytechnique Fédérale de Lausanne, Lausanne, Switzerland. [2]Institute of Materials Science & Engineering, École Polytechnique Fédérale de Lausanne, Lausanne, Switzerland. [3]Department of Cell Biology and Bone Marrow Transplantation Center of the First Affiliated Hospital, Zhejiang University School of Medicine, Hangzhou, China. [4]Department of Oncology, University of Lausanne, Lausanne, Switzerland. [5]Swiss Institute of Bioinformatics, Lausanne, Switzerland. [6]Present address: Institute of Drug Metabolism and Pharmaceutical Analysis, College of Pharmaceutical Sciences, Zhejiang University, Hangzhou, China. [7]National Key Laboratory of Advanced Drug Delivery and Release Systems, Zhejiang University, Hangzhou, China. [8]These authors contributed equally: Yang Zhao, Jiangqing Chen. e-mail: sunj4@zju.edu.cn; yugang.guo@zju.edu.cn; li.tang@epfl.ch

in tumor-infiltrating T cells[7,8]. In addition, impairing mitochondrial oxidative phosphorylation (OXPHOS) suppresses T cell proliferation and promotes exhaustion[9]. Strategies sustaining mitochondrial fitness and respiration, such as antioxidant treatment, could restore the proliferation and effector functions of exhausted T cells[7,8]. CAR T cells cultured in medium supplemented with cytokines, such as engineered interleukin-2 (IL-2) or IL-15, exhibited improved metabolic fitness and enhanced antitumor immunity in vivo when transferred to treat tumor-bearing mice[10,11]. However, it remains challenging to modulate T cell metabolism in vivo and rejuvenate exhausted T cells in the tumor microenvironment (TME).

We recently reported that in vivo administration of an IL-10–Fc fusion protein reprograms intratumoral T cell metabolism toward OXPHOS and increases mitochondrial respiratory capacity, leading to potently enhanced expansion and effector function of terminally exhausted $CD8^+$ tumor-infiltrating lymphocytes (TILs)[12]. This metabolic reprogramming strategy could therefore be exploited to engineer metabolically armored CAR T cell therapy to better treat solid tumors. Here, we show that CAR T cells engineered to express IL-10 prevented the functional impairment associated with T cell exhaustion in the TME, leading to enhanced proliferative capacity and effector function. Further analyses revealed that IL-10 expression improved mitochondrial fitness and increased OXPHOS in CAR T cells in a mitochondrial pyruvate carrier (MPC)-dependent manner. Infusion of mouse and human IL-10-expressing CAR T cells eradicated established solid tumors in multiple syngeneic and xenograft mouse models, respectively, and induced stem cell-like memory (T_{scm} cell) responses to control tumor recurrence. The metabolically armored CAR T cell is a promising therapeutic strategy to counter T cell exhaustion-associated dysfunction and induce potent and long-term antitumor immunity.

Results

IL-10-expressing CAR T cells counter dysfunction in tumors

Adoptive transfer of CAR T cells against human epidermal growth factor receptor 2 (HER2) failed to control established solid tumors partially due to functional impairment of tumor-infiltrating CAR T cells, which exhibited reduced cytotoxicity and higher expression levels of inhibitory receptors than the transferred CAR T cells found in spleen (Extended Data Fig. 1a–e). To counter T cell dysfunction in the TME, we produced a mouse IL-10-expressing HER2 CAR T cell (IL-10 HER2 CAR T) using a tandem construct encoding the second-generation anti-HER2 CAR and mouse IL-10 linked with a cleavable 2A peptide sequence (Fig. 1a). IL-10 HER2 CAR T cells expressed approximately the same levels of CAR as HER2 CAR T cells (Extended Data Fig. 1f) but secreted a high level of IL-10 in the culture (Extended Data Fig. 1g). The secreted IL-10 showed negligible impact on the phenotypes and viability of CAR T cells during the ex vivo preparation phase before infusion (Extended Data Fig. 1h–q).

We next intravenously (i.v.) transferred IL-10 HER2 CAR T cells (3×10^6) or HER2 CAR T cells (3×10^6) in the presence or absence of i.v.-administered free mouse IL-10 to treat established subcutaneous (s.c.) HER2-expressing MC38 (MC38-HER2) mouse colon adenocarcinoma tumors in a mouse model (Fig. 1b). Compared to conventional CAR T cells, IL-10 HER2 CAR T cells exhibited an ~5.3-fold increase in cell counts, augmented Ki67 expression and increased expansion of the population that secretes IL-2 in the tumor, suggesting that IL-10 expression markedly enhanced CAR T cell proliferation (Fig. 1c–e). Consistent with previous reports[12], the PD-1^+TIM-3^+ terminally exhausted subset was notably expanded, whereas the counts of progenitor exhausted T cells (TCF-1^+PD-1^+TIM-3^-) remained unchanged (Fig. 1f and Extended Data Fig. 2a). IL-10 secretion enhanced cytotoxicity and polyfunctionality of HER2 CAR T cells, including both terminally and progenitor exhausted subsets (Fig. 1g,h and Extended Data Fig. 2b,c). IL-10 HER2 CAR T cells also exhibited reduced expression levels of PD-1, suggesting alleviated exhaustion (Fig. 1i). By contrast, secreted IL-10 showed negligible effects on other immune cells or tumor-infiltrating endogenous T cells, including regulatory T (T_{reg}) cells (Extended Data Fig. 2d–g). HER2 CAR T cells with the highest CAR expression density showed decreased cytokine production and increased PD-1 and TIM-3 expression (Fig. 1j–l and Extended Data Fig. 2h,i), suggesting that strong antigen stimulation through CAR may drive exhaustion of intratumoral CAR T cells[13,14]. The extent of functional restoration of IL-10 HER2 CAR T cells by IL-10 secretion seemed dependent on CAR signaling; the reinvigoration of exhausted CAR T cells was in general more prominent when there was a higher CAR density. Of note, we found that delivery of IL-10 through CAR T cell secretion was superior to i.v. administration in reinvigorating exhausted CAR T cells (Fig. 1c–l), likely because secreted IL-10 was enriched in tumors and predominantly acted on tumor-infiltrating CAR T cells.

To extend this strategy to human CAR T (hCAR T) cells, we prepared IL-10-expressing CD19-targeted T cell antigen receptor-α constant (*TRAC*)-deficient hCAR T cells (CD19 hCAR; Extended Data Fig. 3a,b). IL-10 CD19 hCAR T cells secreted human IL-10 in culture and showed enhanced tumor-lytic potential against CD19-expressing PANC1 human pancreatic tumor cells (PANC1-CD19) and Raji lymphoma cells in vitro (Extended Data Fig. 3c–e). After multiple rounds of CAR stimulation by CD19-expressing NIH/3T3 or PANC1-CD19 cells in long-term culture, IL-10 CD19 hCAR T cells exhibited increased expansion compared to conventional CD19 hCAR T cells (Extended Data Fig. 3f,g). Similar to mouse CAR T cells, IL-10 CD19 hCAR T cells that were transferred (i.v.) to immune-deficient NOD *scid* gamma (NSG) mice bearing PANC1-CD19 tumors showed enhanced production of granzyme B and interferon-γ (IFNγ) compared to conventional CD19 hCAR T cells (Fig. 1m–o). Together, incorporation of IL-10 secretion countered CAR T cell dysfunction in tumors by promoting their proliferation and effector function.

IL-10-expressing CAR T cells sustain mitochondrial fitness

Impaired mitochondrial fitness has been shown to reinforce T cell exhaustion[8,15]. We next examined the mitochondrial mass and membrane potential of CAR T cells by staining them with MitoTracker Green (MG) and MitoTracker Deep Red (MDR), respectively. Consistent with prior reports of TILs[8], we found that CAR T cells with dysfunctional

Fig. 1 | IL-10-expressing CAR T cells counter dysfunction in tumors. **a**, Schematic depicting the HER2 CAR and IL-10 HER2 CAR constructs; scFv, single-chain variable fragment; TM, transmembrane domain; LTR, long terminal repeat. **b**–**l**, C57BL/6 mice were inoculated s.c. with MC38-HER2 mouse colon adenocarcinoma cells (1×10^6) and sublethally lymphodepleted by irradiation on day 5 and received i.v. adoptive transfer of IL-10 HER2 CAR T cells (3×10^6) or HER2 CAR T cells (3×10^6) in the presence or absence of i.v.-administered IL-10 (1 μg) on day 6 ($n = 5$ mice; data are pooled from two independent experiments). On day 14, mice were killed, and the indicated tissues were processed and analyzed by flow cytometry. **b**, Experimental timeline. **c**, Counts of viable HER2 CAR T cells in tumors. **d**, Frequencies of Ki67$^+$ HER2 CAR T cells in tumors. **e**–**h**, Counts of viable IL-2$^+$ (**e**), PD-1$^+$TIM3$^+$ (**f**), granzyme B$^+$ (**g**) and polyfunctional (**h**) HER2 CAR T cells in tumors. **i**, Representative flow cytometry plots and average mean fluorescence intensity (MFI) showing PD-1 expression levels on HER2 CAR T cells in tumors. **j**–**l**, CAR T cells in tumors were classified into several subpopulations based on gating of CAR density (**j**). Shown are curves of the MFI of IFNγ (**k**) and PD-1 (**l**) as a function of CAR density. **m**–**o**, NSG mice were inoculated s.c. with PANC1-CD19 cells (5×10^6) and received i.v. adoptive transfer of CD19 hCAR T cells or IL-10 CD19 hCAR T cells (1×10^6; $n = 5$ mice). On day 38, mice were killed, and the indicated tissues were processed and analyzed by flow cytometry. **m**, Experimental timeline. **n**,**o**, Frequencies of granzyme B$^+$ (**n**) and IFNγ$^+$ (**o**) hCAR T cells in tumors. All data represent the mean ± s.e.m. and were analyzed by two-tailed Student's *t*-test (**n** and **o**) or one- or two-way analysis of variance (ANOVA) with Tukey's multiple-comparisons tests (**c**–**i**, **k** and **l**). Data are representative of two independent experiments.

https://doi.org/10.1038/s41587-023-02060-8

mitochondria (defined as a low ratio of MDR to MG; MDR/MG^{lo}) were notably enriched in tumors compared to in the spleen (Fig. 2a,b). The MDR/MG^{lo} subpopulation was substantially less active in degranulation and expressed much higher levels of PD-1 and TIM-3 than the MDR/MG^{hi} population, showing an exhaustion phenotype (Extended Data Fig. 4a). Further, analysis of mitochondrial ultrastructure by electron

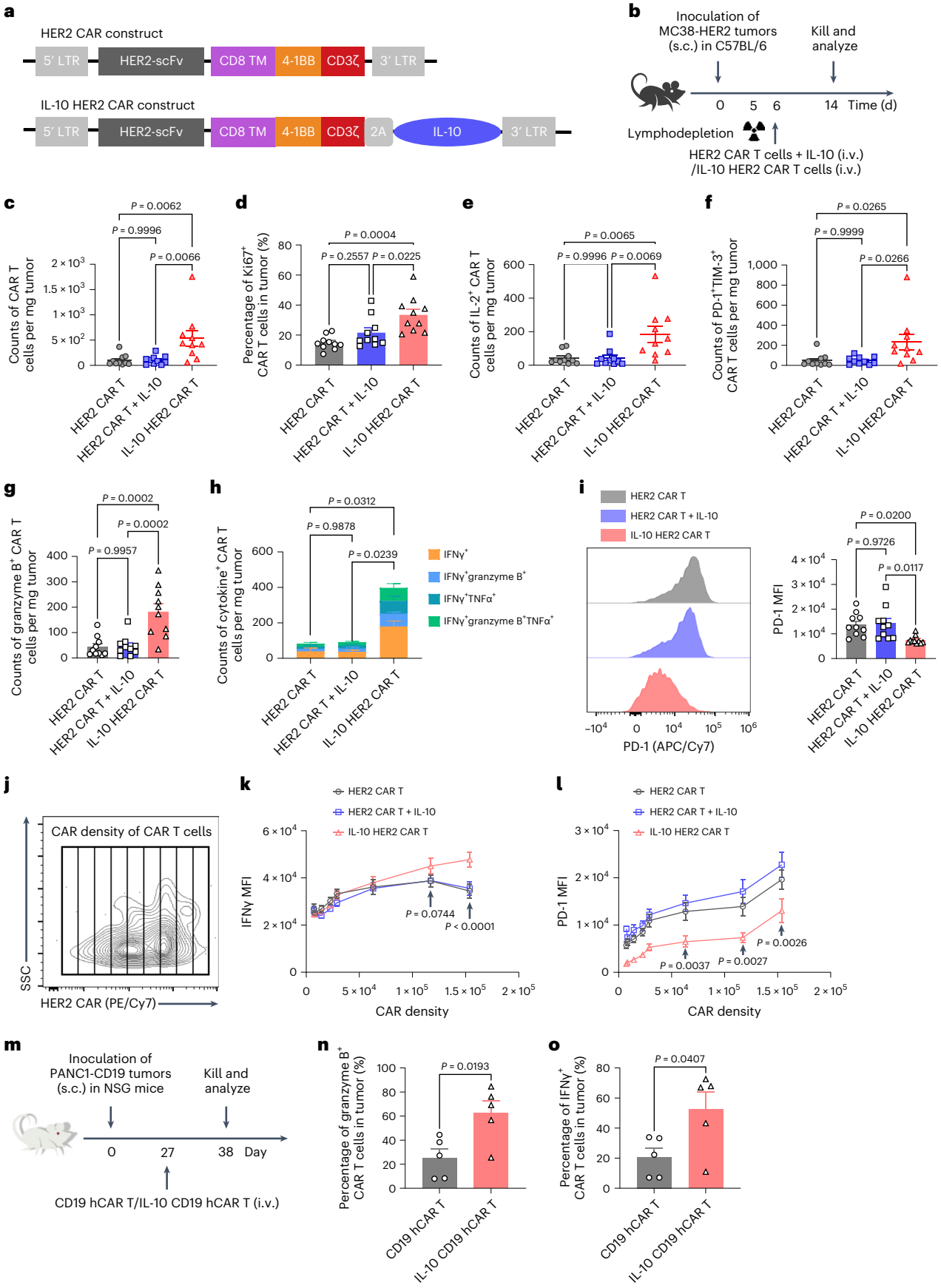

microscopy (EM) indicated that CAR T cells in tumors possessed mitochondria with an enlarged balloon-like shape and loosely structured cristae, whereas splenic CAR T cells exhibited tubular mitochondria with tight cristae (Fig. 2c). In addition, mitochondria in tumor-infiltrating CAR T cells showed reduced crista numbers per mitochondrion and decreased length of cristae per mitochondrial area compared to those in the spleen (Fig. 2d,e). These data reveal the accumulation of dysfunctional mitochondria in exhausted CAR T cells in tumors.

IL-10 expression sustained mitochondria fitness in tumor-infiltrating CAR T cells, with substantially reduced frequencies of dysfunctional mitochondria in IL-10 HER2 CAR T cells (5.5%) compared to HER2 CAR T cells alone (22.9%) and HER2 CAR T cells combined with exogenous IL-10 (23.5%; Fig. 2f,g). IL-10 expression also increased the ratio of MDR to MG in IL-10 HER2 CAR T cells (Fig. 2h). EM imaging analysis of mitochondrial ultrastructure provided additional evidence of enrichment of mitochondria with a tubular shape, well-structured cristae, and increased number and length of cristae in tumor-infiltrating IL-10 HER2 CAR T cells compared to the conventional HER2 CAR T cells (Fig. 2i–l and Extended Data Fig. 4b). HER2 CAR T cells with increased CAR expression density exhibited a higher frequency of dysfunctional mitochondria, which was considerably reduced in IL-10 HER2 CAR T cells (Fig. 2m and Extended Data Fig. 4c). Similarly, IL-10 CD19 hCAR T cells exhibited decreased frequency of cells with dysfunctional mitochondria and an increased ratio of MDR to MG in tumors compared to CD19 hCAR T cells (Fig. 2n,o). These results together suggest that antigen stimulation may drive mitochondrial dysfunction in CAR T cells, whereas IL-10 expression could sustain mitochondrial fitness of CAR T cells, especially those experiencing strong antigen stimulation.

IL-10 expression promotes OXPHOS of CAR T cells

We next assessed whether IL-10 expression could reprogram CAR T cell metabolism. To mimic persistent tumor antigen stimulation in the TME, we cocultured MC38-HER2 cells and HER2 CAR T cells with or without IL-10 expression. After antigen stimulation, IL-10 HER2 CAR T cells exhibited markedly elevated basal and maximal oxygen consumption rates (OCRs) compared to HER2 CAR T cells alone (Fig. 3a,b), whereas extracellular acidification rate (ECAR) remained almost unchanged (Extended Data Fig. 4d,e). Therefore, IL-10 expression increased the ratios of OCR to ECAR and reprogrammed CAR T cell metabolism (Fig. 3c). Addition of exogenous IL-10 also increased the basal OCR of HER2 CAR T cells (Fig. 3b). Notably, in the absence of antigen stimulation, neither exogenous nor secreted IL-10 had any effects on the OCR of CAR T cells (Extended Data Fig. 4f). In addition, metabolomic analysis confirmed that intratumoral IL-10 HER2 CAR T cells exhibited a distinct metabolomic profile compared to conventional HER2 CAR T cells, with markedly increased levels of the pyruvate production intermediate phosphoenolpyruvate and the tricarboxylic acid cycle intermediate succinate (Extended Data Fig. 4g–j and Supplementary Table 1). These results indicate that IL-10 expression reprograms CAR T cell metabolism toward OXPHOS in an antigen-dependent manner.

We recently showed that IL-10–Fc promotes OXPHOS in terminally exhausted $CD8^+$ TILs through MPC[12]. Consistently, by blocking pyruvate transportation using an MPC inhibitor UK5099, but not by inhibiting fatty acid oxidation with etomoxir, we could completely abrogate the increase of OXPHOS in IL-10 HER2 CAR T cells (Fig. 3d). In the coculture with MC38-HER2 cells, IL-10 HER2 CAR T cells exhibited greatly enhanced proliferation, polyfunctionality and killing efficiency of target cells compared to HER2 CAR T cells (Fig. 3e–g), which was consistent with the in vivo results described earlier. Inhibition of MPC-dependent OXPHOS substantially diminished the enhancement of proliferation and polyfunctionality of IL-10 HER2 CAR T cells (Extended Data Fig. 4k,l), suggesting that elevated mitochondrial OXPHOS is necessary for reinvigoration of exhausted CAR T cells. Furthermore, we used *Mpc1*-knockout (*Mpc1*-KO) T cells to generate IL-10 HER2 CAR T cells, which exhibited increased frequencies of accumulated dysfunctional mitochondria and reduced ratios of OCR to ECAR compared to IL-10 HER2 CAR T cells generated from wild-type (WT) T cells (Fig. 3h–j). Moreover, *Mpc1*-KO IL-10 HER2 CAR T cells failed to induce improved proliferation, polyfunctionality or tumor cell-killing capacity compared to WT IL-10 HER2 CAR T cells (Fig. 3k–m). Collectively, we show that IL-10 expression promotes OXPHOS metabolism of CAR T cells in an MPC-dependent manner, which is essential for rejuvenating exhausted CAR T cells with enhanced proliferative capacity and effector function.

IL-10 expression alters transcription of CAR T cells

To investigate the impact of IL-10 expression on CAR T cell fate in the TME at the transcriptional level, we performed a single-cell RNA-sequencing (scRNA-seq) analysis of freshly sorted HER2 CAR T or IL-10 HER2 CAR T cells from MC38-HER2 tumors (Extended Data Fig. 5a). After unsupervised clustering, four distinct clusters were identified based on their gene expression profiles (Fig. 4a and Extended Data Fig. 5b). Notably, cluster 1 was dominantly enriched in IL-10 HER2 CAR T cells, whereas HER2 CAR T cells were mostly found in cluster 0 (Fig. 4b,c). Projection of these scRNA-seq data into a reference atlas of TILs using ProjecTILs[16] revealed that the majority of CAR T cells were mapped to the $CD8^+$ terminally exhausted T cell subtype (Extended Data Fig. 5c). However, compared to cluster 0, cluster 1 displayed higher expression of cytotoxic and effector molecules, including *Gzmb*, *Gzmc*, *Prf1*, *Gzmf* and *Ifng*, as well as transcription factors *Jun*, *Junb* and *Fos* (Fig. 4d,e and Extended Data Fig. 5d). Gene set enrichment analysis (GSEA) between these two clusters indicated that cluster 1 was strongly associated with mitochondrial OXPHOS (Fig. 4f and Extended Data Fig. 5d). Consistent with our previous observation that IL-10–Fc enhanced mitochondrial respiration via pyruvate, we found that cluster 1 showed an enriched pyruvate metabolism pathway compared to cluster 0 (Fig. 4f). In addition, cluster 2, a cluster associated with high expression levels of cell proliferation and cycling genes (Fig. 4d and Extended Data Fig. 5d), was also enriched in IL-10 HER2 CAR T cells (Fig. 4a–c), suggesting higher proliferative capacity of IL-10 HER2 CAR T cells. These results align with our previous observations and suggest

Fig. 2 | IL-10 expression sustains the mitochondrial fitness of CAR T cells. **a**–**m**, The experimental setting was the same as described in Fig. 1b. CAR T cells were subjected to mitochondrial phenotype analysis by flow cytometry ($n = 5$ mice; data were pooled from two independent experiments) or sorted for EM analysis ($n = 15$ biologically independent samples). Mitochondrial mass and membrane potential of CAR T cells were examined by staining with MG and MDR, respectively. **a**, Representative flow cytometry plots showing MDR/MG^{hi} and MDR/MG^{lo} (defined as dysfunctional mitochondria) subpopulations of HER2 CAR T cells in the spleen and tumors. The numbers indicate the frequency (%). **b**, Frequencies of HER2 CAR T cells with dysfunctional mitochondria in the spleen and tumors. **c**, Representative EM images of sorted splenic and intratumoral HER2 CAR T cells. **d**,**e**, Quantification of crista numbers per mitochondrion (**d**) and total crista length per mitochondrial area (**e**) in splenic and intratumoral HER2 CAR T cells. **f**, Representative flow cytometry plots showing dysfunctional mitochondria-enriched CAR T cells in each treatment group. The numbers indicate the frequency (%). Data are representative of two independent experiments. **g**, Frequencies of CAR T cells with dysfunctional mitochondria. **h**, The ratio of MDR/MG in tumor-infiltrating CAR T cells. **i**, Representative EM images of sorted intratumoral CAR T cells. **j**–**l**, Quantification of mitochondrion number per cell (**j**), crista numbers per mitochondrion (**k**) and total crista length per mitochondrial area (**l**) in sorted intratumoral CAR T cells as shown in **i**. **m**, Frequencies of CAR T cells with dysfunctional mitochondria in the subpopulation of different CAR densities. **n**,**o**, The experimental setting was the same as described in Fig. 1m ($n = 5$ mice). **n**, Frequencies of hCAR T cells with dysfunctional mitochondria. **o**, The ratio of MDR/MG in tumor-infiltrating hCAR T cells from the indicated treatment groups. All data represent the mean ± s.e.m. and were analyzed by two-tailed Student's *t*-tests (**b**, **d**, **e** and **j**–**o**) or one-way ANOVA with a Tukey's multiple-comparisons test (**g** and **h**).

https://doi.org/10.1038/s41587-023-02060-8

that IL-10 expression rejuvenates exhausted CAR T cells, sustaining a cell state with enhanced cytotoxicity, effector function and proliferative capacity, which is engaged with metabolic reprogramming toward mitochondrial OXPHOS.

IL-10 CAR T cells eradicate established solid tumors

The discovery that IL-10 HER2 CAR T cells resist dysfunction motivated us to assess their efficacy against solid tumors. In a therapeutic setting of preestablished MC38-HER2 tumors in mice with

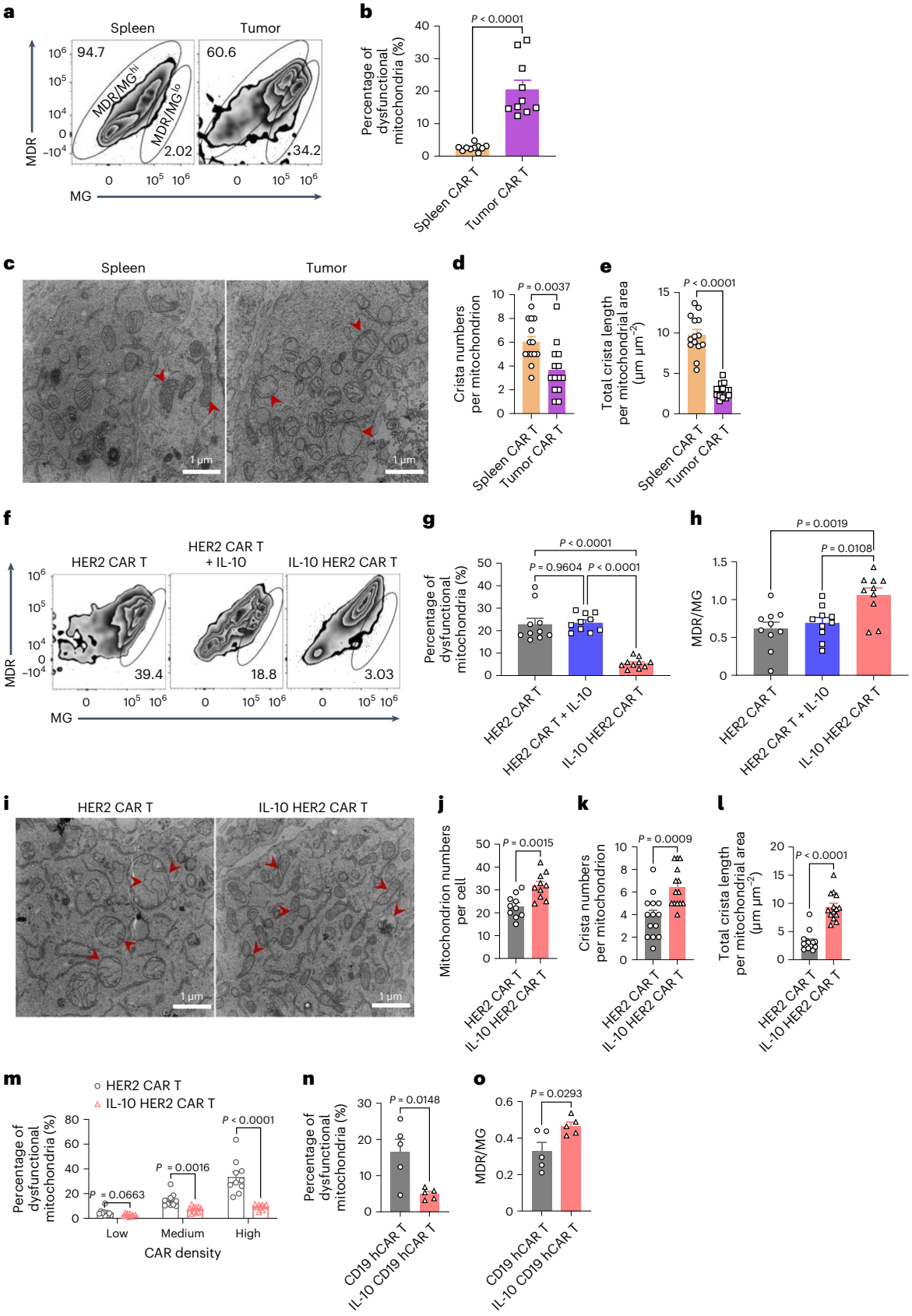

https://doi.org/10.1038/s41587-023-02060-8

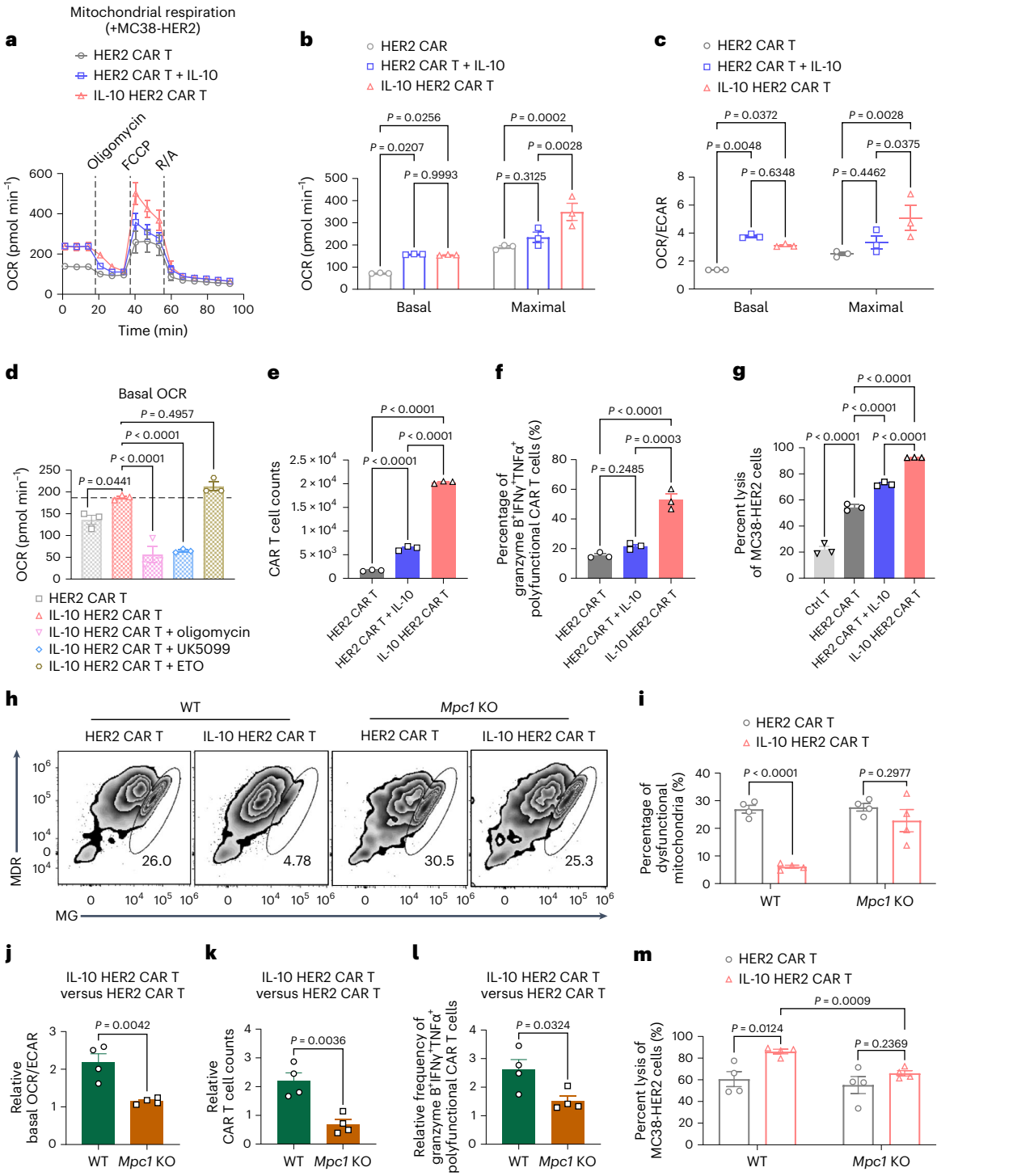

Fig. 3 | IL-10 expression enhances OXPHOS in CAR T cells in an MPC-dependent manner. a–**c**, IL-10 HER2 CAR T cells or HER2 CAR T cells in the presence or absence of IL-10 were cocultured with MC38-HER2 cells at an effector-to-target (E:T) ratio of 5:1 for 18 h. CAR T cells were then isolated for a Seahorse assay ($n = 3$ biologically independent samples). **a**, Real-time analysis of OCR. **b**, Average basal and maximal OCR. **c**, Ratios of basal and maximal OCR to ECAR. **d**, Average basal OCR of IL-10 HER2 CAR T cells in coculture with MC38-HER2 cells (E:T = 5:1) in the presence of different inhibitors ($n = 3$ biologically independent samples); ETO, etomoxir. **e**–**g**, IL-10 HER2 CAR T cells or HER2 CAR T cells in the absence or presence of mouse IL-10 (145 ng ml^{-1}) were cocultured with MC38-HER2 cells at an E:T ratio of 0.5:1 for 48 h ($n = 3$ biologically independent samples). Shown are viable CAR T cell counts (**e**), frequencies of granzyme B$^+$IFNγ$^+$TNFα$^+$ polyfunctional CAR T cells (**f**) and percent lysis of MC38-HER2 cells (**g**); Ctrl T, untransduced T cells. **h**–**m**, HER2 CAR T cells and IL-10 HER2 CAR T cells generated from WT or *Mpc1*-KO T cells were cocultured with MC38-HER2 cells (E:T = 0.5:1) for 48 h. CAR T cells were analyzed by flow cytometry or isolated for a Seahorse assay ($n = 4$ biologically independent samples). **h**, Representative flow cytometry plots showing a dysfunctional mitochondria-enriched subpopulation of CAR T cells in each group. The numbers indicate the frequency (%). **i**, Frequencies of CAR T cells with dysfunctional mitochondria. **j**, Relative ratios of basal OCR to ECAR of WT and *Mpc1*-KO CAR T cells (IL-10 HER2 CAR T cells versus HER2 CAR T cells). **k**, Relative CAR T cell counts of WT and *Mpc1*-KO CAR T cells (IL-10 HER2 CAR T cells versus HER2 CAR T cells). **l**, Relative frequencies of polyfunctional WT and *Mpc1*-KO CAR T cells (IL-10 HER2 CAR T cells versus HER2 CAR T cells). **m**, Percent lysis of MC38-HER2 cells. All data represent the mean ± s.e.m. and were analyzed by two-tailed Student's *t*-tests (**i**–**m**) or one- or two-way ANOVA with a Tukey's multiple-comparisons test (**b**–**g**). Data are representative of two independent experiments.

https://doi.org/10.1038/s41587-023-02060-8

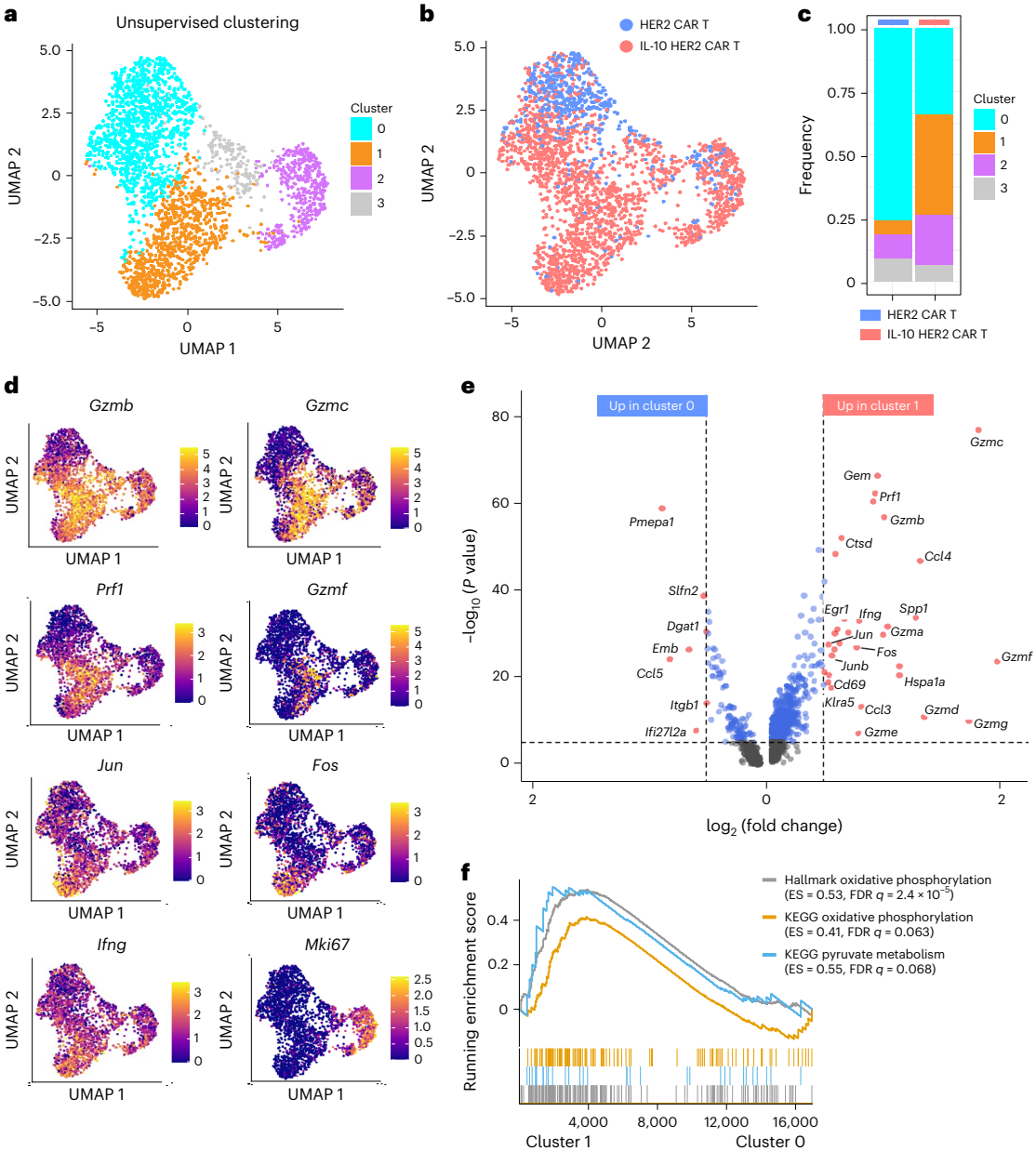

Fig. 4 | IL-10 expression modulates CAR T cell transcription for enhanced cytotoxicity, proliferation and mitochondrial OXPHOS. C57BL/6 mice were inoculated with MC38-HER2 tumor cells (1×10^6, s.c.) and sublethally lymphodepleted by irradiation on day 5 and received i.v. adoptive transfer of HER2 CAR T cells (3×10^6) or IL-10 HER2 CAR T cells (3×10^6) on day 6. On day 18, tumor-infiltrating HER2 CAR T cells or IL-10 HER2 CAR T cells were sorted for scRNA-seq analysis (scRNA-seq samples were pooled from five mice for the HER2 CAR T cell group and six mice for the IL-10 HER2 CAR T cell group). **a**, Uniform manifold approximation and projection (UMAP) of unsupervised cell clusters. **b**, Distribution of HER2 CAR T cells and IL-10 HER2 CAR T cells over the UMAP space. **c**, Cluster composition for HER2 CAR T cells or IL-10 HER2 CAR T cells. **d**, Single-cell expression of key marker genes over the UMAP space. **e**, Volcano plot showing key differentially expressed genes between clusters 1 and cluster 0. Genes with *P* values $<10^{-5}$ and with $\log_2$ (fold change) values of >0.5 are highlighted in red. **f**, GSEA between clusters 1 and 0 of selected signatures from the mSigDB database; ES, enrichment score; FDR, false discovery rate.

lymphodepletion preconditioning, adoptive transfer of IL-10 HER2 CAR T cells (3×10^6) induced complete tumor regression and durable cures in 90% of treated mice (Fig. 5a–c and Extended Data Fig. 6a). By contrast, adoptive transfer of HER2 CAR T cells alone or combined with single or multiple i.v. administrations of native IL-10 transiently controlled tumor growth but failed to induce any durable tumor regression. In fact, treatment with IL-10 HER2 CAR T cells was equivalent to the combination of HER2 CAR T cells and IL-10–Fc (peritumoral injection) and outperformed the combination of HER2 CAR T cells and IL-10–Fc (i.v.) in therapeutic efficacy (Extended Data Fig. 6b–e). No body weight loss or overt elevation in serum cytokines was observed after IL-10 HER2 CAR T cell treatment, suggesting a favorable safety profile (Extended Data Fig. 6f,g). We next extended this strategy to the CAR specific to the melanoma-associated antigen tyrosinase-related protein-1 (TRP-1) and prepared IL-10 TRP-1 CAR T cells (Extended Data Fig. 7a–c). IL-10 TRP-1 CAR T cells exhibited enhanced killing efficiency of TRP-1-expressing B16F10 melanoma cells in vitro compared to conventional TRP-1 CAR T cells (Extended Data Fig. 7d). To treat the poorly immunogenic and highly aggressive mouse B16F10 melanoma tumor, we transferred IL-10 TRP-1 CAR T cells (3×10^6) through i.v. administration, which led to 60% tumor clearance and curative responses in the s.c. tumor model without body weight loss (Fig. 5a,d,e and Extended Data Fig. 7e,f). Furthermore, when applied to treat an orthotopic B16F10 melanoma model, IL-10 TRP-1 CAR T cells induced complete responses in about 40% of treated mice (Extended Data Fig. 7g–j).

We next evaluated whether IL-10-expressing CAR T cells could control metastatic cancer. We prepared epidermal growth factor receptor variant III (EGFRvIII)-targeting CAR T cells with IL-10 expression (Extended Data Fig. 8a–c). Consistent with the finding in HER2 CAR T cells with a 4-1BB endodomain, IL-10 expression also enhanced the basal OCR of CD28-incorporated IL-10 EGFRvIII CAR T cells when cocultured with target cells (Extended Data Fig. 8d). IL-10 EGFRvIII CAR T cells exhibited enhanced in vitro killing efficiency of 4T1 tumor cells that were transduced to express EGFRvIII and luciferase (4T1-EGFRvIII-Luc) compared to EGFRvIII CAR T cells (Extended Data Fig. 8e). To establish a metastasis-like tumor model, BALB/c mice received i.v. injection of 4T1-EGFRvIII-Luc cells. Mice that developed metastatic nodules in the lungs were sublethally lymphodepleted and then received the adoptive transfer of EGFRvIII CAR T cells alone or supported by IL-10 infusion or IL-10 EGFRvIII CAR T cells (Fig. 5a). Tumor growth was monitored by bioluminescence imaging (Fig. 5f). Notably, IL-10 EGFRvIII CAR T cells exhibited superior antimetastasis activity and led to durable cures in 100% of treated mice with no body weight loss, whereas EGFRvIII CAR T cells with or without exogenous IL-10 infusion showed only modest tumor burden control (Fig. 5f–h and Extended Data Fig. 8f). The long-lasting suppression of metastases was likely due to the persistence of IL-10 EGFRvIII CAR T cells in the blood (Extended Data Fig. 8g).

We further extended this therapeutic strategy to hCAR T cells. In immune-deficient mice bearing established s.c. Raji or PANC1-CD19 tumors, transfer of conventional CD19 hCAR T cells (1×10^6) resulted in minimum or transient tumor growth inhibition, respectively, but ultimately failed to control tumor progression (Fig. 5i–l and Extended Data Fig. 9a,b). By contrast, all mice treated with IL-10-expressing CD19 hCAR T cells exhibited complete tumor regression in both models with no recurrence (Fig. 5i–l and Extended Data Fig. 9a,b), suggesting that IL-10-expressing hCAR T cells have superior antitumor capacities against solid tumors in xenograft models. In addition, we established an orthotopic human tumor model of pancreatic ductal adenocarcinoma (PDAC) with PANC1-CD19-Luc tumor cells inoculated in the mouse pancreas (Extended Data Fig. 9c–e). IL-10 CD19 hCAR T cells (1×10^5) eliminated orthotopic PDAC tumors much more effectively than conventional CD19 hCAR T cells (1×10^5), leading to complete responses in 100% of treated mice (Extended Data Fig. 9c–e). Notably, IL-10 CD19 hCAR T cells demonstrated markedly higher expansion after hCAR T cell infusion until at least day 50 (Extended Data Fig. 9f,g). Collectively, these results suggest that IL-10-expressing CAR T cells represent a potent immunotherapy against multiple solid tumors.

IL-10 expression induces stem cell-like memory

To investigate whether IL-10-expressing CAR T cells developed antitumor immune memory, we rechallenged the surviving mice 3 months after adoptive CAR T cell transfer (Extended Data Fig. 10a). All long-term survivors treated with IL-10 HER2 CAR T cells, IL-10 TRP-1 CAR T cells or IL-10 EGFRvIII CAR T cells rejected the second challenge of the original tumor cells (Fig. 6a–c). Similarly, in the human PDAC tumor model, after orthotopic tumor cell rechallenge, all survivors from the treatment group that received IL-10 CD19 hCAR T cells rapidly rejected the second challenge (Extended Data Fig. 9f,h,i). This robust immune memory response motivated us to examine the memory phenotypes of IL-10-expressing CAR T cells in lymphoid tissues and the circulation (Fig. 6d). Flow cytometry analysis of CAR T cells (initially transferred CAR T cells were all $CD44^{hi}$) 12 d after treatment showed that IL-10 HER2 CAR T cells enriched for a population with a T_{scm} cell phenotype (defined as $CD62L^{hi}CD44^{lo}$ and $Sca\text{-}1^{+}CD122^{+}$)[17–20] in the spleen and peripheral blood (Fig. 6e,f and Extended Data Fig. 10b,c). IL-10 HER2 CAR T cells in the spleen showed ~3.2-fold higher frequencies of $CD62L^{hi}CD44^{lo}$ T cells than HER2 CAR T cells alone, among which the majority (~71.2%) were $Sca\text{-}1^{+}CD122^{+}$ T_{scm} cells (Fig. 6e,f). In addition, IL-10 HER2 CAR T cells exhibited substantially increased expression levels of Sca-1 compared to HER2 CAR T cells alone or HER2 CAR T cells plus exogenous IL-10 among all $CD62L^{hi}CD44^{lo}$ CAR T cells (Fig. 6g). Similarly, IL-10 EGFRvIII CAR T cells promoted a higher frequency of T_{scm} cells in the spleen and bone marrow than EGFRvIII CAR T cells (Extended Data Fig. 10e–i). This finding was further confirmed by the observation that IL-10 HER2 CAR T cells were composed of ~3.7- and 2.6-fold higher proportions of $IL\text{-}7R\alpha^{+}KLRG1^{-}$ long-lived memory precursor T cells[21] than HER2 CAR T cells in the spleen and blood, respectively (Fig. 6h and Extended Data Fig. 10d). GSEA confirmed that splenic IL-10 HER2 CAR T cells exhibited a clear transcriptomic state of 'Stemness/Memory' (identified by mouse *Sell*, *Tcf7*, *Lef1*, *Il7r* and *Ccr7*) and were highly enriched for T_{scm} cell-associated genes, including *Id2*, *Ly6a*, *Cxcr3*, *Eomes* and *Bcl2* (Fig. 6i,j and Extended Data Fig. 10j)[22]. Additionally, we observed that, compared to CD19 hCAR T cells, treatment of IL-10 CD19 hCAR T cells appeared enriched with T_{scm} cells, inducing 22.4- and 31.9-fold higher counts of $CD8^{+}$ CAR T cells with a T_{scm} cell phenotype (defined by $CD45RA^{+}CD27^{+}CD62L^{+}CD95^{+}CCR7^{+}$) in the spleen and bone marrow, respectively (Extended Data Fig. 10k–m). Furthermore, scRNA-seq analysis confirmed that IL-10 CD19 hCAR T cells in the spleen had a markedly higher fraction of cells with the gene signature 'Stemness/Memory' (identified by human *TCF7*, *CCR7*, *LEF1* and *SELL*) and expressed higher levels of T_{scm} cell-associated genes, including *IL7R* and *CXCR3*, than conventional CD19 hCAR T cells (Fig. 6k–n and Extended Data Fig. 10n). Together, these results provide clear evidence that IL-10 signaling may induce the formation of mouse and human T_{scm} CAR T cells that contribute to long-term antitumor immunity.

Discussion

Metabolic modulation is a promising strategy to counter T cell dysfunction for improved CAR T cell immunotherapy. Among different strategies, increasing mitochondrial fitness and OXPHOS may be an effective intervention to improve persistence and function of CAR T cells and other adoptive T cell therapies. In the design of second-generation CAR T cells, 4-1BB co-stimulation has been reported to enhance mitochondrial biogenesis and OXPHOS and ameliorate T cell exhaustion and therefore induces better therapeutic outcomes than the CD28 co-stimulatory domain[23,24]. Moreover, preconditioning T cells with IL-15 (ref. 11), coexpressing IL-15 (ref. 25) or deleting *ZC3H12A*[26] could

Fig. 5 | Infusion of IL-10 CAR T cells mediates solid tumor clearance in multiple syngeneic and xenograft models. a–c, C57BL/6 mice were inoculated (s.c.) with MC38-HER2 colon cancer cells (3×10^5) and lymphodepleted and received IL-10 HER2 CAR T cells (3×10^6, i.v.) or HER2 CAR T cells (3×10^6, i.v.) alone or with IL-10 as a single dose (1 μg i.v. on day 6) or multiple doses (3.5 μg i.v. on days 6, 8, 10, 12 and 14; $n = 10$ mice for PBS, HER2 CAR T cells and IL-10 HER2 CAR T cells and $n = 5$ mice for other groups). **a**, Experimental timeline. **b**, Average tumor growth curves. **c**, Survival curves. **d**,**e**, Similar to as shown in **a**. C57BL/6 mice were inoculated (s.c.) with B16F10 melanoma cells (3×10^5) and lymphodepleted and received IL-10 TRP-1 CAR T cells (3×10^6, i.v.) or TRP-1 CAR T cells (3×10^6, i.v.) alone or with IL-10 (1 μg, i.v.) on day 6 ($n = 5$ mice). **d**, Average tumor growth curves. **e**, Survival curves. **f–h**, Similar to as shown in **a**. BALB/c mice were inoculated (i.v.) with 4T1-EGFRvIII-Luc breast cancer cells (5×10^4) and lymphodepleted and received IL-10 EGFRvIII CAR T cells (3×10^6, i.v.) or EGFRvIII CAR T cells (3×10^6, i.v.) alone or with IL-10 (1 μg, i.v.) on day 6 ($n = 5$ mice). **f**, Bioluminescent imaging. **g**, Individual radiance ($p\ s^{-1}\ cm^{-2}\ sr^{-1}$). **h**, Survival curves. **i–l**, NSG mice were inoculated s.c. with Raji lymphoma cells (1×10^6) or PANC1-CD19 human pancreatic tumor cells (2×10^6) and received CD19 hCAR T cells or IL-10 CD19 hCAR T cells (1×10^6, i.v.) on day 8 ($n = 5$ mice for the Raji model and $n = 9$ mice for the PANC1-CD19 model). **i**, Experimental timeline. **j**,**k**, Shown are average tumor growth curves (**j**) and survival curves (**k**) of the Raji model. **l**, Tumor growth curves of the PANC1-CD19 model. Indicated are the numbers of tumor-free mice per total number of mice in the group (**c**, **e**, **h**, **k** and **l**). Data are representative of two independent experiments (**d**–**h**). All data represent the mean ± s.e.m. and were analyzed by two-way ANOVA with a Tukey's multiple-comparisons test (**b**, **d**, **g**, **j** and **l**) or log-rank test (**c**, **e**, **h** and **k**).

https://doi.org/10.1038/s41587-023-02060-8

improve antitumor immunity of T cells through enhanced mitochondrial fitness and OXPHOS. Here, we developed metabolically armored IL-10-secreting CAR T cells, which exhibited enhanced proliferation and effector function by sustaining mitochondrial fitness and promoting OXPHOS, leading to complete remission in multiple syngeneic and xenograft solid tumor models. Moreover, IL-10 secretion in CAR T cells induced T_{scm} cell responses in the peripheral blood and spleen, which bestowed durable protection in treated mice against tumor rechallenge.

Although enhancement of pyruvate-dependent OXPHOS was critical for countering CAR T cell dysfunction, OXPHOS activities that rely on other substrates, in particular, fatty acids, can also preserve

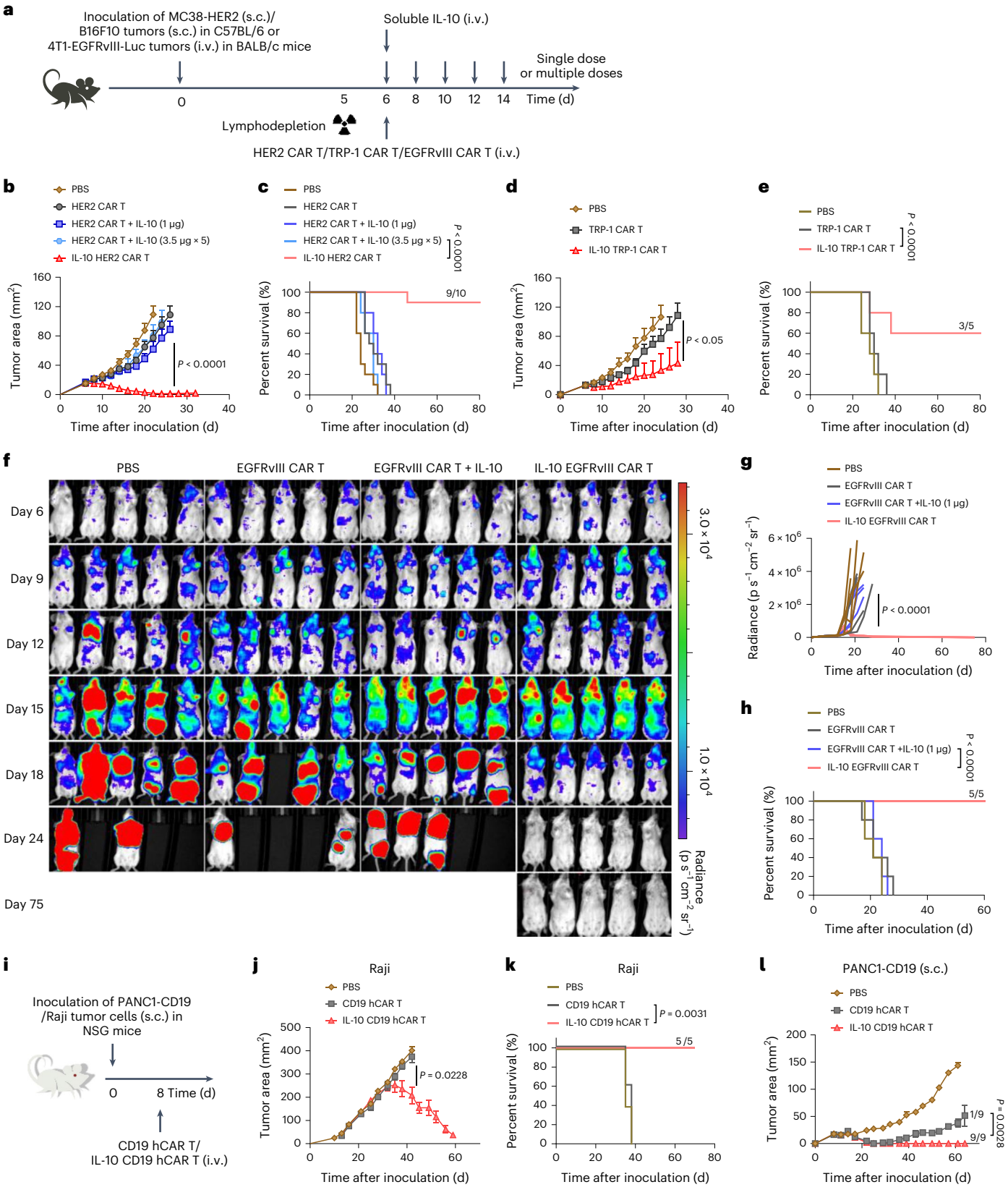

https://doi.org/10.1038/s41587-023-02060-8

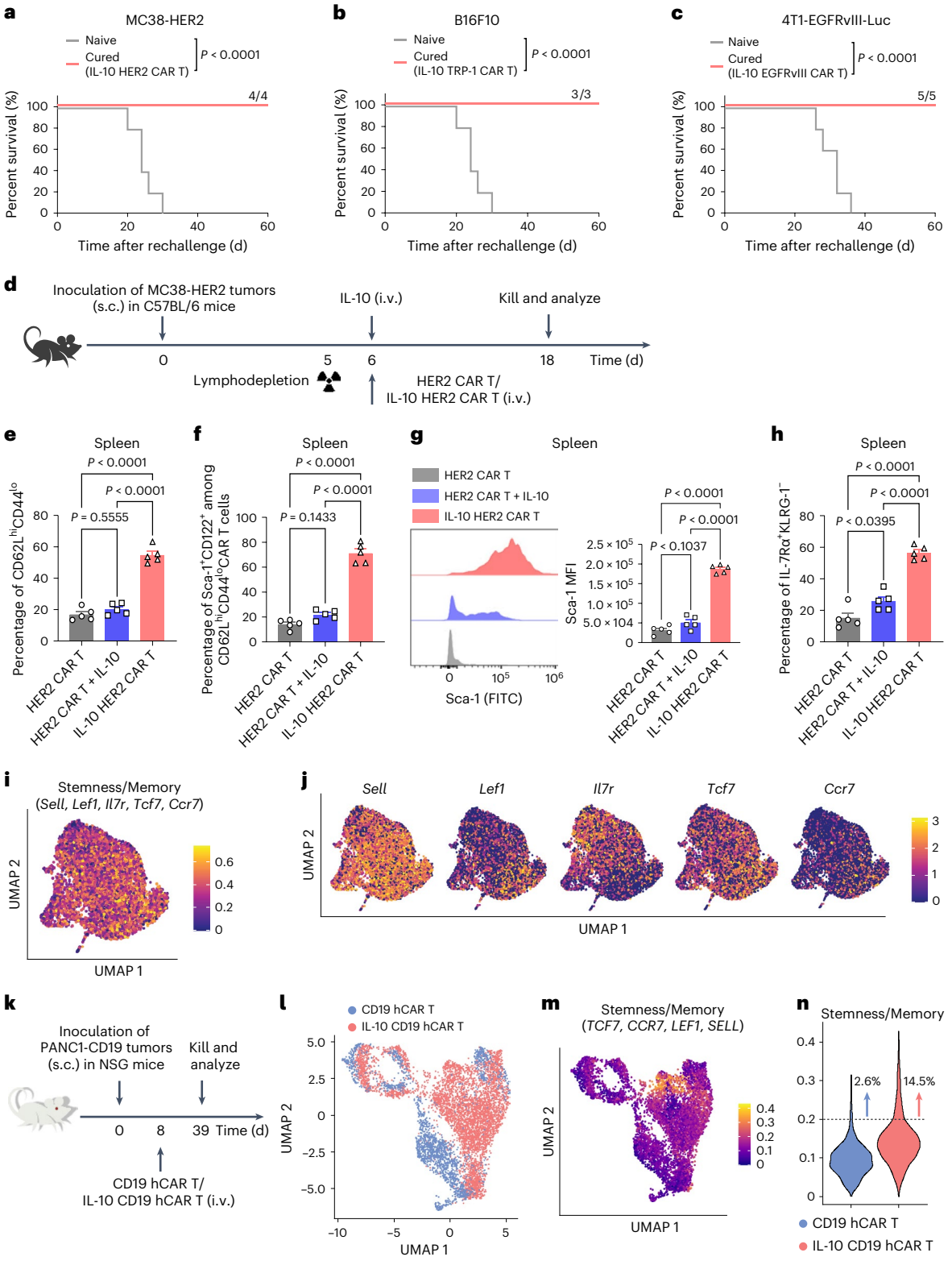

proliferation and function of tumor-infiltrating T cells[27,28]. Therefore, how specific metabolic pathways determine T cell differentiation remains unclear. Recently, it has been reported that CAR T cells engineered to express supporting cytokines[29–31], checkpoint blockade antibody[32] or c-Jun[33] or targeting a CAR to the *TRAC* locus[34] resist exhaustion or dysfunction. Yet, whether and how these strategies alter T cell metabolism remains to be determined. Compared to most existing armored CAR T cells, IL-10 expression in CAR T cells enhanced proliferation and function of terminally exhausted CD8$^+$ T cells (PD-1$^+$TIM-3$^+$), a subset of exhausted T cells that lack responses to other stimulatory cytokines[8] or checkpoint blockades[35] but are direct killers of cancer cells owing to their toxicity[12,35]. Therefore, IL-10 expression complements existing strategies for developing dysfunction-resistant CAR T cell therapy.

We previously showed that multiple local administrations of the half-life-extended IL-10–Fc fusion protein are highly effective in reinvigorating intratumoral exhausted T cells and greatly enhance therapeutic

Fig. 6 | IL-10-expressing CAR T cells confer a memory response against tumor rechallenge and exhibit a stem cell-like memory phenotype in lymphoid organs. Survivors after treatment with IL-10 HER2 CAR T cells, IL-10 TRP-1 CAR T cells and IL-10 EGFRvIII CAR T cells were rechallenged s.c. with MC38-HER2 (1×10^6), B16F10 (1×10^5) and 4T1-EGFRvIII-Luc (5×10^5) cells, respectively, on day 90 after primary tumor inoculation. Naive WT mice ($n = 5$ mice) received an equal number of tumor cells as controls. **a**–**c**, Shown are survival curves of the rechallenged MC38-HER2 (**a**), B16F10 (**b**) and 4T1-EGFRvIII-Luc (**c**) tumor models. Indicated are the numbers of tumor-free mice per total mice in each group. **d**–**j**, C57BL/6 mice were inoculated with MC38-HER2 cells (1×10^6, s.c.) and lymphodepleted and received IL-10 HER2 CAR T cells (3×10^6, i.v.) or HER2 CAR T cells (3×10^6, i.v.) alone or with IL-10 (1 µg, i.v.) on day 6. Mice were killed on day 18 for flow cytometry analysis of CAR T cells in the spleen and blood ($n = 5$ mice) and for scRNA-seq analysis of splenic IL-10 HER2 CAR T cells (samples were pooled from five mice). **d**, Experimental timeline. **e**,**f**, Average frequencies of $CD62L^{hi}CD44^{lo}$ cells among total splenic CAR T cells (**e**) and $Sca\text{-}1^{+}CD122^{+}$ cells among $CD62L^{hi}CD44^{lo}$ CAR T cells (**f**). **g**, Representative flow cytometry plots and Sca-1 MFI among $CD62L^{hi}CD44^{lo}$ splenic CAR T cells. **h**, Frequencies of $IL\text{-}7R\alpha^{+}KLRG1^{-}$ cells among total splenic CAR T cells. **i**, UCell gene signature scores of IL-10 HER2 CAR T cells for the gene set 'Stemness/Memory'. **j**, Single-cell expression of key marker genes over UMAP maps. **k**–**n**, NSG mice were inoculated with PANC1-CD19 cells (2×10^6, s.c.) and received i.v. adoptive transfer of CD19 hCAR T cells or IL-10 CD19 hCAR T cells (1×10^6, i.v.) on day 8. On day 39, mice were killed for scRNA-seq analysis of splenic hCAR T cells (samples were pooled from five mice). **k**, Experimental timeline. **l**, Distribution of hCAR T cells over UMAP maps. **m**, UCell gene signature scores of hCAR T cells for the gene set 'Stemness/Memory'. **n**, Frequencies of hCAR T cells with the 'Stemness/Memory' signature among total hCAR T cells. All data represent the mean ± s.e.m. and were analyzed by one-way ANOVA with a Tukey's multiple-comparisons test (**e**–**h**) or log-rank test (**a**–**c**).

efficacy in combination with adoptive cell therapies, including CAR T cell therapy. Efficient delivery and accumulation of IL-10 in the TME seems crucial because half-life extension through the fusion protein design, local injection and multiple dosages are all required. In this report, we achieved highly efficient intratumoral delivery of IL-10 by engineering CAR T cells with IL-10 expression. CAR T cells secreting a high level of IL-10 likely had the capacity to maintain an effective local concentration of IL-10 in the TME for invigoration of tumor-infiltrating CAR T cells. By contrast, i.v.-administered exogenous recombinant IL-10 (without Fc fusion) of an equivalent dose showed minimal effects on intratumoral T cells in vivo likely due to its short half-life and low level of tumor accumulation. Consequently, a single dose of IL-10-expressing CAR T cells through systemic administration led to equivalent therapeutic efficacy as observed for the combination therapy of CAR T cells in tandem with multiple intratumoral injections of IL-10–Fc[12]. Therefore, using IL-10-expressing CAR T cells as a monotherapy may be a promising future clinical strategy, particularly when intratumoral injection is not feasible.

We found that the heterogeneity of CAR expression density leads to sharp differences in T cell phenotypes, function and extent of responses to secreted IL-10. In general, CAR T cells with higher CAR density expressed higher levels of inhibitory receptors (PD-1 and TIM-3), displayed reduced effector function and responded more prominently to IL-10. These results suggest that strong antigen stimulation signals likely drive T cell exhaustion[3,14]; CAR density may therefore be an important parameter to control in the development of CAR T cells with well-balanced tumoricidal activities and resistance toward antigen stimulation-induced exhaustion and dysfunction[13]. IL-10 was most effective toward the highly exhausted subset with the highest CAR density for metabolic reprogramming and reinvigoration but showed fewer effects in the scenario with low strength of antigen stimulation. These results were in line with the in vitro observation that exogenous or secreted IL-10 failed to enhance OXPHOS in CAR T cells without antigen stimulation. It has been recently reported that IL-10 receptor–STAT3 signaling controls the balance between $PD\text{-}1^{hi}$ exhausted $CD8^{+}$ T cells and functional $PD\text{-}1^{int}TCF\text{-}1^{+}CD8^{+}$ T cells by limiting excessive activation of $CD8^{+}$ T cells[36]. In a microenvironment of low tumor antigen burden, such as the peripheral blood or healthy tissues, secreted IL-10 likely has fewer effects in expanding or activating CAR T cells, thus inducing fewer risks of systemic toxicities. This intrinsic safeguard mechanism could be an additional advantage for IL-10-expressing CAR T cells for potential clinical application.

The IL-10 receptor–STAT3 pathway has been reported to be important for T cell memory formation. IL-10 deficiency leads to a markedly reduced frequency of $KLRG1^{lo}IL\text{-}7R^{hi}$ memory precursor $CD8^{+}$ T cells in acute infection[37]. Furthermore, IL-10 produced from either T_{reg} cells or $CD11c^{+}$ dendritic cells during the resolution of infection promotes the development of $KLRG1^{lo}CD127^{hi}$ and $CD62L^{hi}KLRG1^{lo}$ central memory $CD8^{+}$ T cells[38]. Here, we observed that constitutive expression of IL-10 by CAR T cells induced the loss of CD44 expression, and the majority of IL-10-secreting CAR T cells acquired a stem cell-like memory phenotype ($CD44^{lo}CD62L^{hi}Sca\text{-}1^{+}CD122^{+}$) during tumor clearance. T_{scm} cells possess superior survival capacity, robust proliferative potential after antigen reexposure and the ability to give rise to all memory and effector T cell subsets[18–20]. Promoting stemness is essential for durable protection against relapse with CAR T cell therapy. Additionally, this finding suggests that controlling the strength and persistence of IL-10 signaling may fine-tune CAR T cell differentiation states. Metabolically, memory T cells typically have higher mitochondrial mass and respiration spare capacity[39,40], which is in agreement with our observation that IL-10-expressing CAR T cells have increased mitochondrial activity compared to conventional CAR T cells.

Online content

Any methods, additional references, Nature Portfolio reporting summaries, source data, extended data, supplementary information, acknowledgements, peer review information; details of author contributions and competing interests; and statements of data and code availability are available at https://doi.org/10.1038/s41587-023-02060-8.

References

1. Hou, A. J., Chen, L. C. & Chen, Y. Y. Navigating CAR-T cells through the solid-tumour microenvironment. *Nat. Rev. Drug Discov.* **20**, 531–550 (2021).
2. Blank, C. U. et al. Defining 'T cell exhaustion'. *Nat. Rev. Immunol.* **19**, 665–674 (2019).
3. Wherry, E. J. & Kurachi, M. Molecular and cellular insights into T cell exhaustion. *Nat. Rev. Immunol.* **15**, 486–499 (2015).
4. Wherry, E. J. et al. Molecular signature of $CD8^{+}$ T cell exhaustion during chronic viral infection. *Immunity* **27**, 670–684 (2007).
5. Sen, D. R. et al. The epigenetic landscape of T cell exhaustion. *Science* **354**, 1165–1169 (2016).
6. DePeaux, K. & Delgoffe, G. M. Metabolic barriers to cancer immunotherapy. *Nat. Rev. Immunol.* **21**, 785–797 (2021).
7. Scharping, N. E. et al. Mitochondrial stress induced by continuous stimulation under hypoxia rapidly drives T cell exhaustion. *Nat. Immunol.* **22**, 205–215 (2021).
8. Yu, Y.-R. et al. Disturbed mitochondrial dynamics in $CD8^{+}$ TILs reinforce T cell exhaustion. *Nat. Immunol.* **21**, 1540–1551 (2020).
9. Vardhana, S. A. et al. Impaired mitochondrial oxidative phosphorylation limits the self-renewal of T cells exposed to persistent antigen. *Nat. Immunol.* **21**, 1022–1033 (2020).
10. Mo, F. et al. An engineered IL-2 partial agonist promotes $CD8^{+}$ T cell stemness. *Nature* **597**, 544–548 (2021).
11. Alizadeh, D. et al. IL15 enhances CAR-T cell antitumor activity by reducing mTORC1 activity and preserving their stem cell memory phenotype. *Cancer Immunol. Res.* **7**, 759–772 (2019).

12. Guo, Y. et al. Metabolic reprogramming of terminally exhausted CD8$^+$ T cells by IL-10 enhances anti-tumor immunity. *Nat. Immunol.* **22**, 746–756 (2021).
13. Scarfò, I. & Maus, M. V. Unraveling the signaling balance of activation and exhaustion of CAR T cells. *Cancer Cell* **37**, 143–144 (2020).
14. Mueller, S. N. & Rafi, A. High antigen levels are the cause of T cell exhaustion during chronic viral infection. *Proc. Natl Acad. Sci. USA* **106**, 8623–8628 (2009).
15. Liu, X. & Peng, G. Mitochondria orchestrate T cell fate and function. *Nat. Immunol.* **22**, 276–278 (2021).
16. Andreatta, M. et al. Interpretation of T cell states from single-cell transcriptomics data using reference atlases. *Nat. Commun.* **12**, 2965 (2021).
17. Gattinoni, L. et al. Wnt signaling arrests effector T cell differentiation and generates CD8$^+$ memory stem cells. *Nat. Med.* **15**, 808–813 (2009).
18. Flynn, J. K. & Gorry, P. R. Stem memory T cells (T_{scm})—their role in cancer and HIV immunotherapies. *Clin. Transl. Immunol.* **3**, e20 (2014).
19. Buck, M. D. et al. Mitochondrial dynamics controls T cell fate through metabolic programming. *Cell* **166**, 63–76 (2016).
20. Gattinoni, L. et al. A human memory T cell subset with stem cell-like properties. *Nat. Med.* **17**, 1290–1297 (2011).
21. Herndler-Brandstetter, D. et al. KLRG1$^+$ effector CD8$^+$ T cells lose KLRG1, differentiate into all memory T cell lineages, and convey enhanced protective immunity. *Immunity* **48**, 716–729.e8 (2018).
22. Andreatta, M. & Carmona, S. J. UCell: robust and scalable single-cell gene signature scoring. *Comput. Struct. Biotechnol. J.* **19**, 3796–3798 (2021).
23. Kawalekar, O. U. et al. Distinct signaling of coreceptors regulates specific metabolism pathways and impacts memory development in CAR T cells. *Immunity* **44**, 380–390 (2016).
24. Long, A. H. et al. 4-1BB costimulation ameliorates T cell exhaustion induced by tonic signaling of chimeric antigen receptors. *Nat. Med.* **21**, 581–590 (2015).
25. Hurton, L. V. et al. Tethered IL-15 augments antitumor activity and promotes a stem-cell memory subset in tumor-specific T cells. *Proc. Natl Acad. Sci. USA* **113**, E7788–E7797 (2016).
26. Wei, J. et al. Targeting REGNASE-1 programs long-lived effector T cells for cancer therapy. *Nature* **576**, 471–476 (2019).
27. Zhang, Y. et al. Enhancing CD8$^+$ T Cell Fatty Acid Catabolism within a Metabolically Challenging Tumor Microenvironment increases the Efficacy of Melanoma Immunotherapy. *Cancer Cell* **32**, 377–391.e9 (2017).
28. Chowdhury, P. S., Chamoto, K., Kumar, A. & Honjo, T. PPAR-induced fatty acid oxidation in T cells increases the number of tumor-reactive CD8$^+$ T cells and facilitates anti-PD-1 therapy. *Cancer Immunol. Res.* **6**, 1375–1387 (2018).
29. Ma, X. et al. Interleukin-23 engineering improves CAR T cell function in solid tumors. *Nat. Biotechnol.* **38**, 448–459 (2020).
30. Adachi, K. et al. IL-7 and CCL19 expression in CAR-T cells improves immune cell infiltration and CAR-T cell survival in the tumor. *Nat. Biotechnol.* **36**, 346–351 (2018).
31. Avanzi, M. P. et al. Engineered tumor-targeted T cells mediate enhanced anti-tumor efficacy both directly and through activation of the endogenous immune system. *Cell Rep.* **23**, 2130–2141 (2018).
32. Rafiq, S. et al. Targeted delivery of a PD-1-blocking scFV by CAR-T cells enhances anti-tumor efficacy in vivo. *Nat. Biotechnol.* **36**, 847–858 (2018).
33. Lynn, R. C. et al. c-Jun overexpression in CAR T cells induces exhaustion resistance. *Nature* **576**, 293–300 (2019).
34. Eyquem, J. et al. Targeting a CAR to the *TRAC* locus with CRISPR/Cas9 enhances tumour rejection. *Nature* **543**, 113–117 (2017).
35. Miller, B. C. et al. Subsets of exhausted CD8$^+$ T cells differentially mediate tumor control and respond to checkpoint blockade. *Nat. Immunol.* **20**, 326–336 (2019).
36. Hanna, B. S. et al. Interleukin-10 receptor signaling promotes the maintenance of a PD-1 ^{int}TCF-1$^+$CD8$^+$ T cell population that sustains anti-tumor immunity. *Immunity* **54**, 2825–2841.e10 (2021).
37. Cui, W., Liu, Y., Weinstein, J. S., Craft, J. & Kaech, S. M. An interleukin-21–interleukin-10–STAT3 pathway is critical for functional maturation of memory CD8$^+$ T cells. *Immunity* **35**, 792–805 (2011).
38. Laidlaw, B. J. et al. Production of IL-10 by CD4$^+$ regulatory T cells during the resolution of infection promotes the maturation of memory CD8$^+$ T cells. *Nat. Immunol.* **16**, 871–879 (2015).
39. Bordon, Y. IL-15 provides breathing space for memory. *Nat. Rev. Immunol.* **12**, 77 (2012).
40. Li, W. & Zhang, L. Rewiring mitochondrial metabolism for CD8$^+$ T cell memory formation and effective cancer immunotherapy. *Front. Immunol.* **11**, 1834 (2020).

Methods

Ethics statement

Experiments and handling of mice in syngeneic tumor models were conducted under federal, state and local guidelines with approval from the Swiss authorities (Canton of Vaud, animal protocol IDs 3206 and 3533) and performed in accordance with the guidelines from CPG of EPFL and the animal facility of University of Lausanne. Human peripheral blood mononuclear cells were received from healthy volunteers with written informed consent, and the protocol was approved by the Ethics Committee of Zhejiang University School of Medicine (no. 2020-003). All NSG mouse experiments in xenograft models were approved by the Institutional Animal Care and Use Committee of Zhejiang University (animal protocol no. 20220178).

Mice

Five- to 6-week-old female C57BL/6 (C57BL/6J) mice and BALB/c (BALB/cByJ) mice were purchased from Charles River Laboratories. Six- to 12-week-old NOD-*scid*/*Il2rg*^{null} (NSG) mice were purchased from GemPharmatech. T cell antigen receptor-transgenic OT-I mice (C57BL/6-Tg(TcraTcrb)1100Mjb/J) were originally purchased from Jackson Laboratory and maintained in the École Polytechnique Fédérale de Lausanne (EPFL) Center of PhenoGenomics (CPG) animal facility. *Mpc1*$^{fl/fl}$ mice were crossed to *Cd4*^{cre} mice on an OT-I background to generate *Mpc1*-KO OT-I mice. Experimental procedures in mouse studies were approved by the Swiss authorities (Canton of Vaud, animal protocol IDs 3206 and 3533) and Institutional Animal Care and Use Committee of Zhejiang University (animal protocol no. 20220178) and were performed in accordance with the guidelines from the CPG of EPFL, the animal facility of University of Lausanne and Zhejiang University.

Cells and tumor models

HER2-transduced MC38 mouse colon cancer cells (MC38-HER2), CD19-expressing PANC1 epithelioid cells (PANC1-CD19) and CD19-expressing NIH/3T3 cells (NIH/3T3-CD19) were generated according to previous publications[41,42]. B16F10 melanoma cells, Phoenix-Eco cells and Raji cells were originally acquired from ATCC, and 4T1-EGFRvIII-Luc mouse breast cancer cells were provided by D. J. Irvine (Massachusetts Institute of Technology). All mouse tumor cells and PANC1-CD19 and NIH/3T3-CD19 cells were cultured in complete DMEM (DMEM (Gibco/Thermo Fisher Scientific) supplemented with 10% (vol/vol) fetal bovine serum (FBS; Gibco/Thermo Fisher Scientific) and 1% (vol/vol) penicillin/streptomycin (Gibco/Thermo Fisher Scientific)). Raji cells were maintained in RPMI-1640 supplemented with 10% (vol/vol) FBS (Gibco/Thermo Fisher Scientific) and 1% (vol/vol) penicillin/streptomycin (Gibco/Thermo Fisher Scientific). MC38-HER2 (3×10^5) and B16F10 tumor cells (3×10^5) were implanted s.c. into the right flanks of C57BL/6 WT mice to establish the syngeneic s.c. tumor models. B16F10 tumor cells (2×10^5) were also implanted intradermally into the right flanks of C57BL/6 WT mice to establish the syngeneic orthotopic melanoma model. 4T-EGFRvIII-Luc tumor cells (5×10^4) were injected i.v. into BALB/c WT mice. PANC1-CD19 tumor cells (2×10^6) and Raji tumor cells (1×10^6) were inoculated s.c. into the right flanks of NSG mice to establish the xenograft tumor models. PANC1-CD19-Luc tumor cells (2×10^6) were orthotopically implanted into the tails of the pancreas of NSG mice to establish an orthotopic PDAC model.

Construction of mouse and human CARs

CAR constructs targeting HER2 were generated as previously described[41]. Briefly, the complete HER2 CAR sequence was composed of a mouse CD8 signal peptide, antigen-specific scFv (4D5 scFv), mouse CD8α hinge and transmembrane domain, 4-1BB co-stimulatory domain and CD3ζ intracellular domain. Constructs for CARs targeting TRP-1 and EGFRvIII were provided by D. J. Irvine. The complete CAR sequence was composed of a mouse CD8 signal peptide, antigen-specific scFv (TA99 scFv for monospecific TRP-1 CAR and 139scFv for EGFRvIII CAR), mouse CD8a hinge and transmembrane domain, CD28 co-stimulatory domain and CD3ζ intracellular domain. To facilitate CAR detection by flow cytometry, a c-Myc tag was inserted between the scFv and CD8α hinge for the EGFRvIII CAR and TRP-1 CAR. The CD19 hCAR comprised an scFv specific for human CD19 preceded by a CD8α leader peptide and followed by CD28 hinge–transmembrane–intracellular regions and a CD3ζ intracellular domain, as described in previous publications[34]. Full-length mouse *Il10* (accession number NP_034678.1) and human *IL10* (accession number NM_000572.2) were amplified by PCR from cDNA clones custom purchased from Twist Bioscience and Genescript, respectively. IL-10 CAR constructs were generated by fusing 2A self-cleaving peptide and *Il10* gene fragments into the CAR containing viral vector (pMSGV for HER2 CAR, pMSCV for TRP-1 CAR and EGFRvIII CAR and pAAV for CD19 hCAR).

Retrovirus production

Retrovirus production was performed using the calcium phosphate method following the manufacturer's protocol (Clonetech). Briefly, Phoenix cells were seeded in a 10-cm dish and cultured for 18 h before transfection and replenished with 10 ml of prewarmed medium without disturbing the cells before transduction. For each transfection, 14 μg of plasmid (8.5 μg of CAR plasmid plus 5.5 μg of pCL-Eco packaging plasmid) was added to 628 μl of ultrapure water, followed by the addition of 72 μl of a $CaCl_2$ solution (2 M; Sigma-Aldrich). HEPES buffered saline (700 μl × 2; Sigma-Aldrich) was then added in a dropwise manner with gentle vortexing. After a 20-min incubation at 25 °C, the transfection mixture was gently added to Phoenix cells and replenished with 10 ml of prewarmed medium 16 h later. After 36–72 h of incubation, virus-containing supernatant was collected and passed through a 0.45-μm filter (Merck Millipore) to remove cell debris. Virus-containing supernatant was then aliquoted and stored at −80 °C.

Preparation of mouse CAR T cells

Spleens from WT OT-I mice were disintegrated mechanically and filtered through a 70-μm strainer (Fisher Scientific). Red blood cells (RBCs) were lysed with ACK lysis buffer (2 ml per spleen; Gibco/Thermo Fisher Scientific) for 5 min at 25 °C. The splenocytes were washed once with cold complete RPMI medium (RPMI-1640 (Gibco), FBS (10% (vol/vol); Gibco/Thermo Fisher Scientific), HEPES (1% (vol/vol); Gibco/Thermo Fisher Scientific), penicillin/streptomycin (1% (vol/vol); Gibco/Thermo Fisher Scientific), sodium pyruvate (1% (vol/vol); Gibco/Thermo Fisher Scientific) and 2-mercaptoethanol (0.1% (vol/vol); Gibco/Thermo Fisher Scientific)) and resuspended at a cell density of 2×10^6 cells per ml in complete RPMI medium supplemented with IL-2 (10 ng ml^{-1}; PeproTech) and IL-7 (10 ng ml^{-1}; PeproTech). For WT T cell activation, six-well plates were precoated with 1 ml of anti-CD3 (1 μg ml^{-1}; 17A2, BioXCell) and anti-CD28 (5 μg ml^{-1}; 37.51, BioXCell) per well at 4 °C for 18 h. OT-I T cells were activated with $OVA_{257–264}$ peptide (1 μM; GenScript). T cells were enriched by using Ficoll-Paque PLUS (GE Healthcare) and seeded onto precoated six-well plates at 3×10^6 cells per well in complete RPMI medium (3 ml per well). Cells were cultured at 37 °C for 48 h without disturbance. Six-well plates were coated with protamine (10 μg ml^{-1}; Sigma-Aldrich) for 24 h before transduction. On day 2, protamine-coated plates were blocked with FBS (0.5% (vol/vol)) containing PBS for 30 min before use. Virus supernatant was added into each well of the blocked plates (1 ml per well), and plates were centrifuged at 2,000*g* for 2 h at 32 °C. Activated T cells were collected, enriched again by using Ficoll-Paque PLUS and resuspended at 2×10^6 cells per ml in complete RPMI medium supplemented with IL-2 (10 ng ml^{-1}). The cell suspension described above was added to virus-enriched plates (1 ml per well) and mixed by gentle shaking; spin transfection was performed at 500*g* for 30 min at 32 °C. Plates were then transferred to an incubator and maintained overnight. A second transduction was conducted on day 3, and T cells were collected and added into virus-containing plates after centrifugation. After overnight

incubation, T cells were collected and expanded in fresh complete RPMI medium supplemented with IL-2 (10 ng ml^{-1}). On day 5, the transduction efficiency was determined by flow cytometry analyses. For HER2 CAR T cells, CAR expression was detected by using a biotinylated human HER2/ERBB2 protein (ACROBiosystems) and the secondary staining reagent Streptavidin-PE/Cyanine7 (BioLegend). TRP-1 CAR or EGFRvIII CAR expression was evaluated by surface staining of the c-Myc tag using anti-Myc (9B11, Cell Signaling). Untransduced T cells activated and cultured in parallel with virus-free medium were used as a control. CAR T cells were used on day 6 for both in vitro and in vivo experiments.

Generation of hCAR T cells

Peripheral blood was obtained from healthy volunteers. All blood samples were handled following the required ethical and safety procedures. Peripheral blood mononuclear cells were isolated by density gradient centrifugation, and T cells were purified using a Pan T Cell Isolation kit (Miltenyi Biotec). T cells were then stimulated with CD3/CD28 T cell Activator Dynabeads (Thermo Fisher Scientific) and cultured in X-VIVO 15 serum-free medium (Lonza) supplemented with FBS (10% (vol/vol); HyClone), penicillin/ streptomycin (1% (vol/vol); HyClone), human IL-7 (5 ng ml^{-1}; Novoprotein) and human IL-15 (5 ng ml^{-1}; Novoprotein). Human T cells were stimulated for 48 h and debeaded for gene targeting experiments. Gene targeting experiments were performed as described previously[34]. In short, modified guide RNA (C*A*G*GGUUCUGGAUAUCUGU; * represents 2′-O-methyl 3′ phosphorothioate) targeting the first exon of the constant chain of the *TRAC* gene was synthesized by Genescript. Cas9 protein was purified from *Escherichia coli* strain Rosetta by using a heparin column and a Superdex 200 increase column on an AKTA Pure system (GE Healthcare), as described previously[43]. Adeno-associated viruses containing the CAR gene were produced by Vigene Biosciences. Ribonucleoprotein complexes were produced by complexing two components: guide RNA and Cas9 protein. Stimulated human T cells were incubated with ribonucleoprotein complexes for 15 min at room temperature, and adeno-associated viruses were added (multiplicity of infection = 1×10^5) within 20 min after electroporation. After a 16-h incubation, cells were continually cultured, and medium was changed every 2 d. On day 7 after electroporation, cells were collected for flow cytometry analysis to determine the CAR knock-in efficiency, and supernatant was collected to determine human IL-10 concentration with a Cytometric Bead Array kit (BD Biosciences).

Flow cytometry analyses

For surface marker staining, cells were collected into U-bottom, 96-well plates (Thermo Fisher Scientific), blocked with anti-mouse CD16/32 (BioLegend) and incubated with the indicated antibodies at 4 °C for 20 min, followed by live/dead staining with DAPI (Sigma-Aldrich). Cells were then washed and resuspended with PBS containing bovine serum albumin (BSA; 0.2% (wt/vol); Sigma-Aldrich) for flow cytometry analyses. For mitochondrial staining, cells were stained with MG (100 nM; Thermo Fisher Scientific) and MDR (10 nM; Thermo Fisher Scientific) for 20 min at 37 °C for mitochondrial mass and membrane potential assessments, respectively. Afterward, cells were further stained for surface markers and DAPI for flow cytometry analyses. For intracellular cytokine staining, cells were first stimulated with Cell Stimulation Cocktail (Invitrogen/Thermo Fisher Scientific) at 37 °C for 5 h. After stimulation, cells were stained for surface markers and with Zombie Aqua Fixable Dye (BioLegend) and fixed and permeabilized with a Cytofix/Cytoperm Fixation/Permeabilization Solution kit (BD Biosciences). Intracellular staining with the indicated antibodies was performed following the manufacturer's protocol. Cells were detected using an Attune NxT Flow Cytometer with Attune NxT Software v.3 (Invitrogen/Thermo Fisher Scientific) or an LSRFortessa with FACSDiva Software (BD Biosciences). Analyses were performed using FlowJo 10.8.1 (Tree Star). Gate margins were determined by isotype controls and fluorescence minus one controls.

Antibodies and reagents for flow cytometry

The following antibodies or staining reagents were purchased from BioLegend: CD16/32 (93, 101302), CD45.2 (104, 109814), CD8β (YTS256.7.7, 126606), CD4 (RM4-5, 100526), NK1.1 (PK136, 108740), F4/80 (BM8,123108), CD3ε (17A2, 100306), CD11c (N418, 117348), I-A/I-E (MHC-II, M5/114.15.2, 107643), Siglec-F (S17007L, 155508), CD80 (16-10A1, 104734), CD86 (GL-1, 105006), CD11b (M1/70, 101228), Ki67 (16A8, 652424), granzyme B (GB11, 515403), IFNγ (XMG1.2, 505826), TNFα (MP6-XT22, 506308), IL-2 (JES6-5H4, 503822), Gr-1 (RB6-8C5, 202519), PD-1 (29F.1A12, 135216), TIM-3 (RMT3-23, 119706), CD107a (H4A3, 328608), CD44 (IM7, 103028), CD62L (MEL-14, 104432), CD122 (5H4, 105906), Sca-1 (D7, 108106), KLRG1 (2F1/KLRG1, 138410), IL-7Rα (SB/199, 121111), human CD95 (DX2, 305606), Streptavidin-PE/Cyanine7 (405206), human granzyme B (QA16A02, 372208) and human IFNγ (B2, 552887). The following antibodies or staining reagents were purchased from BD Biosciences: human CD4 (SK3, 563550) and human CD8 (SK1, 557834). The following antibodies or staining reagents were purchased from Invitrogen: human CD62L (DREG56, 48-0629-42), human CD45RA (H100, 69-0458-42), human CD27 (O323, 56-0279-42) and CCR7 (3D12, 61-1979-42). Biotinylated human HER2/ERBB2 protein (HE2-H822R) was purchased from ACROBiosystems. Myc tag antibody (9B11, 3739) was obtained from Cell Signaling Technology. Goat anti-mouse IgG was purchased from Jackson ImmunoResearch. MitoTracker Green FM and MitoTracker Deep Red FM were obtained from Thermo Fisher Scientific.

Cytotoxicity assay of hCAR T cells

On day 7 after electroporation, CD19 hCAR T cells and target PANC1-CD19 (5×10^4) or Raji (5×10^4) cells were cocultured in complete RPMI-1640 medium at the indicated E:T ratios using black, 96-well flat plates (Thermo Fisher Scientific). Target cells alone were plated at the same cell density to determine the maximal luciferase expression (relative light units (RLU)). After 18 h of coculture, luciferin (1.5 mg ml^{-1}, 100 µl per well; GoldBio) was added to each well. Luminescence was detected in a plate reader. Percent lysis was determined by using the following equation: $(1 - \mathrm{RLU}_{\mathrm{sample}}/\mathrm{RLU}_{\mathrm{max}}) \times 100\%$.

Antitumor therapy and rechallenge experiments

C57BL/6 or BALB/c WT mice bearing established tumors were sublethally lymphodepleted by total body irradiation (4 Gy) on day 5. On day 6, mice received i.v. adoptive transfer of CAR T cells (HER2 CAR T cells, TRP-1 CAR T cells or EGFRvIII CAR T cells, 3×10^6 CAR$^+$ T cells) in the presence or absence of a single dose of i.v.-administered IL-10 (1 µg) on day 6, multiple doses of IL-10 (3.5 µg, equivalent to 20 µg of IL-10–Fc[12]) or multiple doses of IL-10–Fc (20 µg five times) through i.v. or peritumoral administration on days 6, 8, 10, 12 and 14; IL-10 CAR T cells (IL-10 HER2 CAR T cells, IL-10 TRP-1 CAR T cells or IL-10 EGFRvIII CAR T cells, 3×10^6 CAR$^+$ T cells); untransduced T cells (equivalent total number of cells infused) or PBS. For the MC38-HER2 or B16F10 tumor model in C57BL/6 mice, tumor area and body weight were measured every other day. For the s.c. PANC1-CD19 tumor model and the Raji tumor model, NSG mice received i.v. adoptive transfer of CD19 hCAR T cells (1×10^6 CAR$^+$ T cells) or IL-10 CD19 hCAR T cells (1×10^6 CAR$^+$ T cells) on day 8 after tumor inoculation. For the orthotopic PANC1-CD19-Luc tumor model, NSG mice received i.v. adoptive transfer of CD19 hCAR T cells (1×10^5 CAR$^+$ T cells) or IL-10 CD19 hCAR T cells (1×10^5 CAR$^+$ T cells) on day 4 after tumor inoculation. For the s.c. tumor model, tumor area was calculated by the formula area = length × width from caliper measurements of two orthogonal diameters. For the 4T1-EGFRvIII-Luc metastatic tumor model and orthotopic PDAC model, mice were anesthetized and intraperitoneally injected with bioluminescent substrate D-luciferin potassium salt (100 µl; GoldBio) prediluted at 30 mg ml^{-1} in 1× PBS. Ten minutes after injection, mice were subjected to luminescent imaging using a Xenogen IVIS fluorescence/bioluminescence imaging system or Photon Imager (Biospace Lab) for tumor growth

monitoring. In tumor cell rechallenge experiments in the syngeneic model, MC38-HER2 (1×10^6), B16F10 (1×10^5) and 4T1-EGFRvIII-Luc (5×10^5) cells were reinoculated s.c. into the left flanks of mice that survived from treatment groups 3 months after adoptive CAR T cell transfer. Naive WT mice were s.c. inoculated with the same number of tumor cells as the control group. In the tumor cell rechallenge experiments in the xenograft model, PANC1-CD19-Luc (2×10^6) cells were orthotopically inoculated into the pancreas tail of mice that survived from treatment groups 46 d after adoptive CAR T cell transfer. Naive NSG mice were orthotopically inoculated with the same number of tumor cells as the control group. Survival of rechallenged mice was monitored for at least another 60 d. Mice were killed when body weight loss was beyond 15% of baseline weight, tumor area reached 150 mm^2 (mouse syngeneic models) or the maximum diameter reached 20 mm (NSG mouse models) or if any signs of discomfort were detected by the investigators or as recommended by the veterinarian who monitored the mice every other day.

Analyses of tumor-infiltrating immune cells and serum cytokines

C57BL/6 mice were inoculated s.c. with MC38-HER2 tumor cells (1×10^6) and sublethally lymphodepleted by irradiation on day 5 and received i.v. adoptive transfer of HER2 CAR T cells (3×10^6 CAR^+ T cells) in the presence or absence of i.v.-administered IL-10 (1 µg), IL-10 HER2 CAR T cells (3×10^6 CAR^+ T cells) or PBS control on day 6 after tumor inoculation. On day 14, mice were killed, and tumors and sera were collected. NSG mice were inoculated s.c. with PANC1-CD19 cells (5×10^6) and received i.v. adoptive cell transfer of CD19 hCAR T cells or IL-10 CD19 hCAR T cells (1×10^6). On day 27, mice were killed, and tumors were collected. Collected tumors were weighed, mechanically minced and digested in RPMI-1640 medium supplemented with collagenase type IV (1 mg ml^{-1}; Gibco/Thermo Fisher Scientific), dispase II (100 µg ml^{-1}; Sigma-Aldrich), hyaluronidase (100 µg ml^{-1}; Sigma-Aldrich) and DNase I (100 µg ml^{-1}; Sigma-Aldrich) at 37 °C for 60 min. RBC lysis was performed on the digested tumor samples with ACK lysing buffer. TILs were then enriched by Percoll (GE Healthcare) density gradient centrifugation, resuspended in PBS with 0.2% BSA (wt/vol), stained with the indicated antibodies and analyzed by flow cytometry. Serum was collected from C57BL/6 mice and analyzed by enzyme-linked immunosorbent assay (ELISA) using the ELISA MAX Standard Set for mouse IL-1β, IL-2, IL-6 and IFNγ (BioLegend) to determine the serum concentrations of the indicated cytokines.

Analyses of CAR T cells from spleen, blood and bone marrow

For the MC38-HER2 model, C57BL/6 mice were inoculated s.c. with MC38-HER2 tumor cells (1×10^6) and sublethally lymphodepleted by irradiation on day 5 and received i.v. adoptive transfer of HER2 CAR T cells (3×10^6 CAR^+ T cells) in the presence or absence of i.v.-administered IL-10 (1 µg), IL-10 HER2 CAR T cells (3×10^6 CAR^+ T cells) or PBS control on day 6 after tumor inoculation. On day 18, spleens and blood were collected for phenotypic analyses of CAR T cells. For the 4T1-EGFRvIII-Luc model, BALB/c mice were inoculated i.v. with 4T1-EGFRvIII-Luc tumor cells (5×10^4) and sublethally lymphodepleted by irradiation on day 5 and received i.v. adoptive transfer of EGFRvIII CAR T cells (3×10^6 CAR^+ T cells) in the presence or absence of i.v.-administered IL-10 (1 µg), IL-10 EGFRvIII CAR T cells (3×10^6 CAR^+ T cells) or PBS control on day 6 after tumor inoculation. On days 6, 9, 12, 15 and 18, mice were bled to monitor CAR T cell counts in the blood. For the PANC1-CD19 model, NSG mice were inoculated s.c. with PANC1-CD19 cells (2×10^6) and received i.v. adoptive cell transfers of CD19 hCAR T cells (1×10^6 CAR^+ T cells) or IL-10 CD19 hCAR T cells (1×10^6 CAR^+ T cells) on day 8. On day 63, mice were killed for phenotypic analyses of CAR T cells in the spleen and bone marrow. For the PANC1-CD19-Luc model, NSG mice were orthotopically implanted with PANC1-CD19-Luc cells (2×10^6) and received i.v. adoptive cell transfers of CD19 hCAR T cells (5×10^5 CAR^+ T cells) or IL-10 CD19 hCAR T cells (5×10^5 CAR^+ T cells) on day 4. On days 18, 28 and 50, blood samples were collected and subsequently analyzed by flow cytometry to assess the expansion of CAR T cells in the blood. Spleens were dissected from the surrounding tissues, ground and filtered through a 70-µm strainer (Fisher Scientific). RBC lysis was performed on the spleen samples with ACK lysing buffer (2 ml per spleen; Gibco/Thermo Fisher Scientific) and resuspended in PBS with BSA (0.2% (wt/vol)). Blood samples were resuspended in PBS with ethylenediaminetetraacetic acid (2 mM; Invitrogen). RBCs were lysed with ACK lysis buffer, debris was removed by Percoll (GE Healthcare), and cells were resuspended in PBS with 0.2% BSA (wt/vol). Bone marrow was collected from freshly isolated femurs and tibiae. Bones were crushed in 5 ml of PBS with ethylenediaminetetraacetic acid (2 mM; Sigma-Aldrich) and filtered with strainers. Remaining RBCs were lysed with ACK buffer. Collected cells from the samples described above were stained with the indicated antibodies and analyzed by flow cytometry.

Cell sorting

Splenic IL-10 HER2 CAR T cells, tumor-infiltrating HER2 CAR T cells or IL-10 HER2 CAR T cells from the MC38-HER2 tumor model were enriched by density gradient centrifugation against Percoll (GE Healthcare) and stained with surface markers and DAPI (Sigma-Aldrich), followed by sorting with an Aria II sorter (BD Biosciences) at the EPFL Flow Cytometry Core Facility. Splenic CD19 hCAR T cells or IL-10 CD19 hCAR T cells from the PANC1-CD19 tumor model were enriched by using a human CD45 isolation MACS kit (Miltenyi Biotec) and stained with surface markers and DAPI (Sigma-Aldrich), followed by sorting with an Aria II sorter at the FACS facility at Zhejiang University.

Electron microscopy

Sorted HER2 CAR T cells or IL-10 HER2 CAR T cells were fixed for 1 h in 2.5% glutaraldehyde (vol/vol; Sigma-Aldrich) and 1% formaldehyde (vol/vol; Sigma-Aldrich) in sodium cacodylate buffer (0.12 M; Sigma-Aldrich). Cell sections were prepared by the EPFL Biological Electron Microscopy Facility. Ultrathin sections (50 to 60 nm) were obtained using a Leica EM UC7 ultramicrotome. Sections were examined with a Talos L120C TEM for Life Sciences (Thermo Fisher Scientific) at an accelerating voltage of 80 keV. Mitochondrial parameters were measured by using Fiji imaging software (ImageJ).

In vitro coculture of CAR T cells and tumor cells

MC38-HER2, B16F10 or 4T1-EGFRvIII-Luc tumor cells (1×10^5 cells per well) were seeded in 12-well plates (Thermo Fisher Scientific) in complete DMEM and incubated overnight. After aspiration of tumor culture medium, HER2 CAR T cells, TRP-1 CAR T cells or EGFRvIII CAR T cells on day 6, as described above, were suspended in complete RPMI supplemented with IL-2 (10 ng ml^{-1}) and added to the tumor cell culture at an E:T ratio of 0.5:1 in the presence or absence of IL-10 (145 ng ml^{-1}). After another 2-d coculture, cells in the plates were collected, and flow cytometry analyses were conducted to determine the tumor cell viability and the proliferation and phenotypes of CAR T cells. IL-10 concentration in the culture supernatants was determined by an ELISA MAX Standard Set Mouse IL-10 kit (BioLegend) after 3 d of coculture.

In vitro restimulation of hCAR T cells with tumor cells

Seven days after electroporation, CAR T cells were cocultured with irradiated NIH/3T3-CD19 or PANC1-CD19 cells for weekly restimulation. Typically, NIH/3T3-CD19 or PANC1-CD19 cells (1.25×10^5) were plated on 24-well tissue culture plates 12 h before the addition of CAR T cells (5×10^5) in X-VIVO 15 serum-free medium (Lonza) supplemented with 10% (vol/vol) FBS, 1% (vol/vol) penicillin/ streptomycin, 5 ng ml^{-1} human IL-7 and 5 ng ml^{-1} human IL-15. Every week, the total number of cells were counted using Countstar Rigel S2 (Alit Biotech). CAR expression was detected by flow cytometry.

Seahorse assay

MC38-HER2 tumor cells (1×10^6 cells per flask) were seeded in T25 flasks (Thermo Fisher Scientific) in complete DMEM and incubated overnight. After aspiration of tumor cell culture medium, HER2 CAR T cells (WT, OT-I or *Mpc*-KO OT-I) cells or IL-10 HER2 CAR T cells (WT, OT-I or *Mpc*-KO OT-I) in complete RPMI medium supplemented with IL-2 (10 ng ml^{-1}) were added to the tumor cell culture at an E:T ratio of 5:1. In some experiments, the medium was supplemented with IL-10 (145 ng ml^{-1}) or various inhibitors as indicated. After 16 h of coculture, CAR T cells in the flasks were collected and isolated by Ficoll-Paque PLUS for the Seahorse assay. Seahorse assays were performed to measure OCR and ECAR of CAR T cells. CAR T cells (3×10^5 cells per well) with different treatment conditions were seeded in a Seahorse culture plate (Seahorse Bioscience) in a non-CO_2 incubator at 37 °C for 40 min. OCR and ECAR were measured with a Seahorse XFe96 Analyzer (Seahorse Bioscience) following the manufacturer's instructions. During a Seahorse assay, cells were treated with oligomycin (1 µM; Sigma-Aldrich), carbonyl cyanide-4-(trifluoromethoxy)phenylhydrazone (2 µM; Sigma-Aldrich), rotenone (0.5 µM; Sigma-Aldrich), antimycin A (0.5 µM; Sigma-Aldrich), glucose (10 mM; Sigma-Aldrich) and 2-deoxy-D-glucose (50 mM; Sigma-Aldrich). Each condition was performed with three to five replicates in a single experiment. Basal or maximal OCR and ECAR were calculated according to previous reports[44].

Metabolic inhibitor treatments

MC38-HER2 cells (1×10^5 cells per well) were seeded on 12-well plates (Thermo Fisher Scientific) and incubated overnight. HER2 CAR T cells or IL-10 HER2 CAR T cells on day 6, as described above, were cocultured with preseeded MC38-HER2 cells at an E:T ratio of 0.5:1 in complete RPMI medium containing IL-2 (10 ng ml^{-1}) and the indicated inhibitors (oligomysin, 1 µM; UK5099 (Sigma-Aldrich), 100 µM; etomoxir (Sigma-Aldrich), 200 µM) for 2 d. Absolute counts and phenotypes of CAR T cells were determined by flow cytometry analyses.

Metabolomic analyses

Mice bearing MC38-HER2 tumors were sublethally lymphodepleted by total body irradiation (4 Gy) on day 5, followed by i.v. adoptive transfer of HER2 CAR T cells or IL-10 HER2 CAR T cells on day 6. On day 14, mice were killed, and CAR T cells were isolated from tumors as described above. Metabolomic analyses were performed by the University of Lausanne Metabolomics Unit. Cell lysates were preextracted and homogenized by the addition of 200 µl of methanol in a Cryolys Precellys 24 sample homogenizer (2 × 20 s at 10,000 r.p.m.; Bertin Technologies) with ceramic beads. Homogenized extracts were centrifuged for 15 min at 4,000*g* at 4 °C (Hermle). The resulting supernatant was collected and evaporated to dryness in a vacuum concentrator (LabConco). Dried sample extracts were resuspended in methanol:water (4:1 (vol/vol)) according to the total protein content. The protein pellets were evaporated and lysed in Tris-HCl buffer (20 mM, pH 7.5) with guanidine hydrochloride (4 M), NaCl (150 mM), Na_2EDTA (1 mM), EGTA (1 mM), Triton (1%), sodium pyrophosphate (2.5 mM), β-glycerophosphate (1 mM), Na_3VO_4 (1 mM) and leupeptin (1 µg ml^{-1}) using a Cryolys Precellys 24 sample homogenizer (2 × 20 s at 10,000 r.p.m.; Bertin Technologies) with ceramic beads. A BCA Protein Assay kit (Thermo Scientific) was used to measure total protein concentration (adsorption at 562 nm; Hidex). Extracted samples were analyzed by hydrophilic interaction liquid chromatography coupled to tandem mass spectrometry in both positive and negative ionization modes using a 6495 triple quadrupole system interfaced with a 1290 UHPLC system (Agilent Technologies). Pooled quality control (QC) samples were analyzed periodically throughout the overall analytical run to assess the quality of the data, correct the signal intensity drift and remove peaks with poor reproducibility. In addition, a series of diluted QC samples was prepared by dilution with methanol: 100% QC, 50% QC, 25% QC, 12.5% QC and 6.25% QC. Metabolites were then selected also considering the linear response on the diluted QC series. Raw liquid chromatography–tandem mass spectrometry data were processed using Agilent Quantitative analysis software (version B.07.00; MassHunter Agilent Technologies). Relative quantification of metabolites was based on extracted ion chromatogram areas for the monitored multiple reaction monitoring transitions. The obtained tables (containing peak areas of detected metabolites across all samples) were exported to R software (http://cran.r-project.org/). Signal intensity drift correction and noise filtering were done within MRM PROBS software. The preprocessed data with peak areas were imported into Metaboanalyst 5.0 for further data analysis.

scRNA-seq and bioinformatics analyses

MC38-HER2-bearing mice were sublethally lymphodepleted by total body irradiation (4 Gy) on day 5, followed by i.v. adoptive transfer of HER2 CAR T cells or IL-10 HER2 CAR T cells on day 6. On day 18, mice were killed, and CAR T cells were isolated from tumors or spleens as described above. NSG mice were inoculated (s.c.) with PANC1-CD19 cells (2×10^6) and received i.v. adoptive cell transfer of CD19 hCAR T cells or IL-10 CD19 hCAR T cells (1×10^6) on day 8. On day 39, mice were killed, and CAR T cells were isolated from spleens as described above. Sorted HER2 CAR T cells from tumors were then pelleted for 5 min at 400*g* and washed once in PBS with BSA (0.04% (wt/vol)). Afterward, HER2 CAR T cells or IL-10 HER2 CAR T cells were suspended in 100 µl of Cell Multiplexing Oligo (LMO, 10x Genomics). LMO barcode labeling was performed for 10 min at room temperature, and cells were washed twice with PBS, resuspended in PBS with BSA (0.04% (wt/vol)), filtered and pooled. Labeled cells were subjected to single-cell encapsulation using a Chromium Single Cell Instrument and reagents. Sorted CD19 hCAR T cells or IL-10 CD19 hCAR T cells from spleens were subjected to single-cell encapsulation using a Chromium Single Cell Instrument and reagents separately. A Chromium Next GEM Chip G was loaded with the appropriate number of cells, and the sequencing were libraries prepared using 10x Genomics reagents according to the manufacturer's instructions and passed QC. Briefly, an emulsion encapsulating single cells into droplets with reagents and gel beads containing a unique molecular identifier (UMI), reverse transcription reagents and cell barcoding oligonucleotides was generated. cDNAs were obtained and amplified after droplets broke. For the 5′ Gene Expression library, the cDNA was fragmented, ligated to a sequencing adaptor and PCR amplified. The generated 5′ Gene Expression libraries were sequenced using an Illumina HiSeq 4000 with a sequencing depth of 115,000 paired-end reads per cell for HER2 CAR T cells from tumors and a sequencing depth of 46,000 paired-end reads per cell for CD19 hCAR T cells from spleens. The fastq files were generated and demultiplexed by cellranger mkfastq from 10x Genomics (version 3.0.2), and primary data analysis was performed with Cell Ranger (version 2.2.0) using a custom reference package based on the mm10 or GRCh38 reference genome and GENCODE gene models. For IL-10 HER2 CAR T cells from the spleen, cells were subjected to single-cell partitioning using a microchip, and mRNA capture and sequencing libraries were prepared using GEXSCOPE Single Cell RNA Library Kit Cell V2 reagents (Singleron Biotechnologies) according to the manufacturer's instructions and passed QC. Briefly, single partitioning was performed by loading single cells into a microchip and loading barcode beads containing a UMI. Cells were lysed, and mRNA capturing beads were retrieved. cDNAs were obtained via reverse transcription, amplified and purified. For the 5′ Gene Expression library, the cDNA was fragmented, ligated to a sequencing adaptor and PCR amplified. The generated 5′ Gene Expression libraries were sequenced using an Illumina HiSeq 4000 with a sequencing depth of 50,000 paired-end reads per cell. The fastq files were generated and demultiplexed by CeleScope rna from Singleron (version 3.0.1), and primary data analysis was performed with CeleScope (version 1.10.0) using a custom reference package based on reference genome Mus_musculus_ensembl_92.

To demultiplex samples of HER2 CAR T cells from tumors based on LMO barcodes, we applied the HTODemux function implemented in Seurat v4.0.5 (ref. 45) using default settings. QC was applied to remove outlier cells with less than 500 or over 50,000 UMI counts, less than 500 or over 6,000 genes and abnormal ribosomal or mitochondrial gene content (over 40% and 7.5%, respectively). To remove potential contaminants or cell doublets, we applied the scGate package v1.0.0 (ref. 46) using a default T cell filter. Dimensionality reduction was performed by calculating ten principal components from 500 variable genes, further reducing dimensionality by UMAP for two-dimensional visualization. Unsupervised clustering was performed on the principal component reduction using the FindNeighbors and FindClusters functions implemented in Seurat with parameters k.param = 30 and resolution = 0.35. Differentially expressed genes between clusters were determined using the FindMarkers function of Seurat, which applies a Wilcoxon test to determine significance. Differentially expressed genes were visualized using the EnhancedVolcano R package (https://github.com/kevinblighe/EnhancedVolcano) with a $\log_2$ (fold change) cutoff of 0.5 and P value of 10^{-5}. Gene sets for relevant biological processes and pathways were obtained from the database mSigDB[47], and signature scores for these gene sets were calculated using the UCell package[22]. GSEA between clusters was performed on average gene expression by cluster using the R package clusterProfiler[48] and relevant signatures from mSigDB[48]. Projection of HER2 CAR T cells or IL-10 HER2 CAR T cells into a reference atlas of TILs was performed using the ProjecTILs method[16] with default parameters.

Statistical analysis

Statistical analysis was performed using GraphPad Prism 9 (GraphPad software) except scRNA-seq data, which were analyzed with R (described above). Metabolomics data (Extended Data Fig. 5h) were imported into MetaboAnalyst 5.0 for further analysis. Data are presented as mean ± s.e.m. unless otherwise indicated. Comparisons of two groups were performed by using two-tailed unpaired Student's t-tests unless otherwise indicated. Comparisons of multiple groups were performed by using a one- or two-way ANOVA with a Tukey's multiple-comparisons test. Survival data were analyzed using log-rank tests. No statistically significant differences were considered when P values were larger than 0.05.

Reporting summary

Further information on research design is available in the Nature Portfolio Reporting Summary linked to this article.

Data availability

All data generated and supporting the findings of this study are available within the paper. scRNA-seq data for the mouse CAR T cells from this study have been deposited in the Gene Expression Omnibus under accession number GSE245517. scRNA-seq data for the hCAR T cells are available in the CNGB Sequence Archive of the China National GeneBank Database under accession number CNP0003547. Source data are provided with this paper. Additional information and materials will be made available upon reasonable request.

Code availability

The R code required to reproduce the scRNA-seq data shown in Figs. 4 and 6 and Extended Data Figs. 5 and 10 is available at the following repository: https://github.com/carmonalab/LiTang_IL10_CART.

References

41. Tschumi, B. O. et al. CART cells are prone to Fas- and DR5-mediated cell death. *J. Immunother. Cancer* **6**, 71 (2018).
42. Brentjens, R. J. et al. Eradication of systemic B-cell tumors by genetically targeted human T lymphocytes co-stimulated by CD80 and interleukin-15. *Nat. Med.* **9**, 279–286 (2003).
43. Jing, R. et al. Cas9-cleavage sequences in size-reduced plasmids enhance nonviral genome targeting of CARs in primary human T cells. *Small Methods* **5**, 2100071 (2021).
44. Michelet, X. et al. Metabolic reprogramming of natural killer cells in obesity limits antitumor responses. *Nat. Immunol.* **19**, 1330–1340 (2018).
45. Hao, Y. et al. Integrated analysis of multimodal single-cell data. *Cell* **184**, 3573–3587.e29 (2021).
46. Andreatta, M., Berenstein, A. J. & Carmona, S. J. scGate: marker-based purification of cell types from heterogeneous single-cell RNA-seq datasets. *Bioinformatics* **38**, 2642–2644 (2022).
47. Liberzon, A. et al. Molecular signatures database (MSigDB) 3.0. *Bioinformatics* **27**, 1739–1740 (2011).
48. Yu, G., Wang, L.-G., Han, Y. & He, Q.-Y. clusterProfiler: an R package for comparing biological themes among gene clusters. *OMICS* **16**, 284–287 (2012).

Acknowledgements

We thank D. J. Irvine (Massachusetts Institute of Technology) for providing TRP-1 CAR and EGFRvIII CAR plasmids and 4T1-EGFRvIII-Luc cells, J. Auwerx (EPFL) for providing access to a Seahorse XFe96 Analyzer, and J. Shi and Y. Wang (Zhejiang University) for technical support for the orthotopic PDAC model. We acknowledge the EPFL CPG, Flow Cytometry Core Facility, Gene Expression Core Facility and Biological Electron Microscopy Facility and the University of Lausanne Center of Metabolomics Platform for technical assistance. We thank Y. Li, Y. Huang and C. Guo from the Core Facilities, Zhejiang University School of Medicine, for their technical support. This work was supported, in part, by the Swiss National Science Foundation (315230_173243, 316030_189686, 315230_204202, IZLCZ0_206035 and CRSII5_205930), Swiss Cancer Research Foundation (KFS-4600-08-2018), Kristian Gerhard Jebsen Foundation, the European Research Council under the ERC grant agreement MechanoIMM (805337), Anna Fuller Fund grant, Xtalpi, Inc., and EPFL. J.S. was funded by the National Natural Science Foundation of China grants 82161138028 and 31971324, Zhejiang Provincial Natural Science Foundation grant LR20H160003 and National Key R&D Program of China grant 2021YFA0909900. S.C. was supported by the Swiss National Science Foundation Ambizione grant 180010. P.R. was supported, in part, by grants from the Swiss National Science Foundation (310030_182735) and the Swiss Cancer League (KFS-4404-02-18). M.G. was supported by the Chinese Scholarship Council (201808320453). X.H. has received funding from the European Union's Horizon 2020 research and innovation programme under the Marie Skłodowska-Curie grant agreement 754354 and was supported by the China Scholarship Council (201700260266).

Author contributions

Y.Z., J.C., J.S., Y.G. and L.T. conceived the study. Y.Z., J.C., J.S., Y.G. and L.T. designed the experiments. Y.Z., J.C., M.A., B.F., Y.-Q.X., M.W., Y.W., M.G., X.H., P.R. and S.C. performed the experiments. Y.Z., J.C., J.S., Y.G. and L.T. analyzed the data and wrote the paper. All authors edited the paper.

Competing interests

Y.G., L.T. and Y.Z. are inventors on patents related to the technology described in this paper. L.T. and Y.G. are cofounders, share-holders and advisors for Leman Biotech. The interests of L.T. were reviewed and managed by EPFL. The other authors declare no competing interests.

Additional information

Extended data is available for this paper at https://doi.org/10.1038/s41587-023-02060-8.

Supplementary information The online version contains supplementary material available at https://doi.org/10.1038/s41587-023-02060-8.

Correspondence and requests for materials should be addressed to Jie Sun, Yugang Guo or Li Tang.

Peer review information *Nature Biotechnology* thanks the anonymous reviewers for their contribution to the peer review of this work.

https://doi.org/10.1038/s41587-023-02060-8

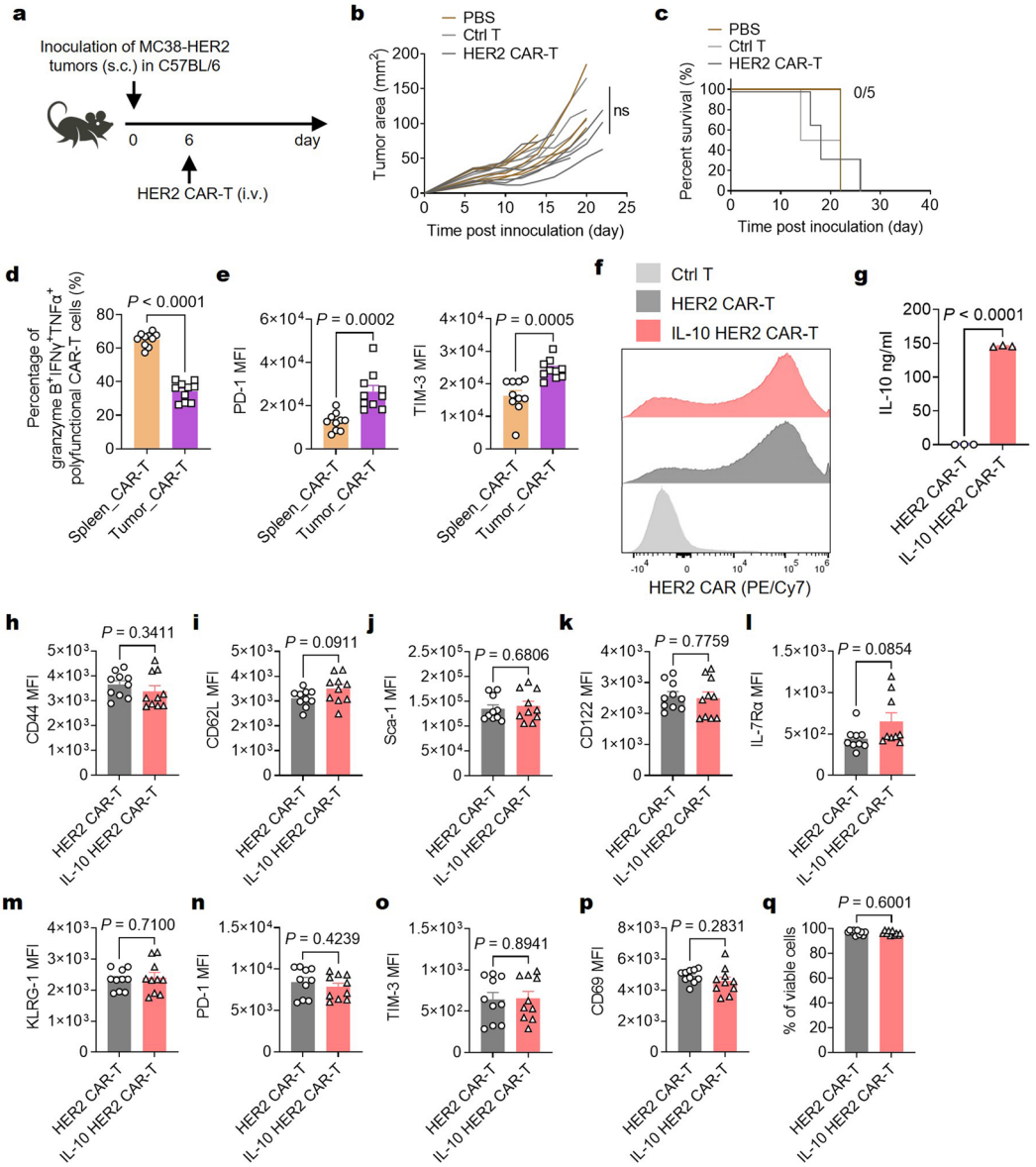

Extended Data Fig. 1 | In vitro characterizations of IL-10 CAR-T cells prior to infusion. a-e, C57BL/6 mice were inoculated subcutaneously (s.c.) with MC38-HER2 colon cancer cells (3×10^5) and received intravenously (i.v.) adoptive cell transfer of HER2 CAR-T cells (3×10^6), untransduced T cells (Ctrl T, equivalent cell number infused), or phosphate buffered saline (PBS) on day 6. Mice were either monitored for tumor growth (n = 5 mice) or sacrificed on day 14 for the analysis of CAR-T cells (n = 10 mice). **a**, Experimental timeline. **b**–**e**, Shown are individual tumor growth curves (**b**), survival curves (**c**), frequencies of granzyme $B^+IFN\gamma^+TNF\alpha^+$ polyfunctional CAR-T cells in spleen and tumor (**d**), and MFI of PD-1 and TIM-3 (**e**). Indicated are numbers of tumor-free mice/total mice in each group (**c**). **f**, HER2 CAR or IL-10 HER2 CAR constructs were introduced via retroviral vectors. CAR expression levels were assessed by flow cytometry. Data are one representative of ten independent experiments. **g**, HER2 CAR-T or IL-10 HER2 CAR-T cells were co-cultured with MC38-HER2 tumor cells for 3 days (n = 3 biologically independent samples)). The culture supernatants were assessed for IL-10 concentration using an enzyme-linked immunosorbent assay (ELISA). **h-q**, CAR-T cells prior to infusion were examined for the expression levels of indicated markers by flow cytometry (n = 9 biologically independent samples for IL-7Rα, and n = 10 biologically independent samples for others). Shown are average MFI of CD44 (**h**), CD62L (**i**), Sca-1 (**j**), CD122 (**k**), IL-7Rα (**l**), KLRG-1 (**m**), PD-1 (**n**), TIM-3 (**o**), and CD69 (**p**) expression in HER2 CAR-T and IL-10 HER2 CAR-T cells. **q**, Average frequencies of viable CAR-T cells. All data represent the mean ± s.e.m. and are analyzed by two-tailed Student's t-test (**d**, **e**, **g-q**), or one- or two-way ANOVA with Tukey's multiple-comparisons test (**b**) or log-rank test (**c**). ns, not significant ($P > 0.05$). Data are one representative of two independent experiments.

https://doi.org/10.1038/s41587-023-02060-8

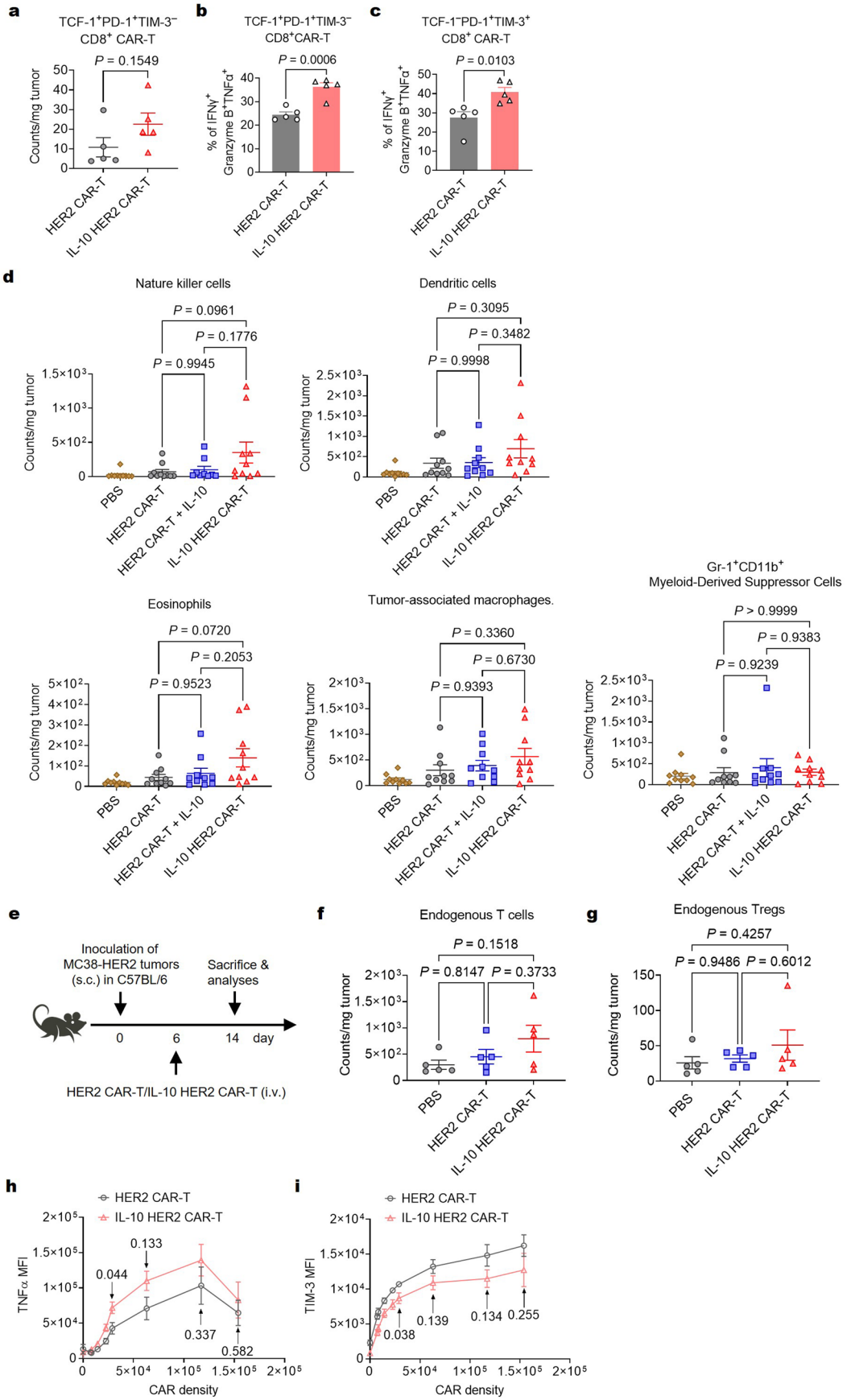

Extended Data Fig. 2 | See next page for caption.

https://doi.org/10.1038/s41587-023-02060-8

Extended Data Fig. 2 | IL-10 expression shows negligible effects on other immune cells or endogenous T cells in tumor. a-**c**, The experimental setting was the same as described in Fig. 1b (n = 5 mice). **a**, Counts of TCF-1$^+$PD-1$^+$TIM3$^-$CD8$^+$ HER2 CAR-T cells in tumors. **b**,**c**, Frequencies of IFNγ$^+$Granzyme B$^+$TNFα$^+$ polyfunctional cells among PD-1$^+$TCF-1$^+$TIM3$^-$ (**b**) and PD-1$^+$TCF-1$^-$TIM3$^+$ (**c**) CD8$^+$ CAR-T cells. **d**, The experimental setting was the same as described in Fig. 1b (n = 10 mice). Counts of indicated immune cell subsets in the MC38-HER2 tumors from each treatment group. **e**-**g**, C57BL/6 mice were inoculated s.c. with MC38-HER2 colon cancer cells (1×10^6) and received i.v. adoptive transfer of IL-10 HER2 CAR-T cells (3×10^6) or HER2 CAR-T cells (3×10^6) on day 6 (n = 5 mice). **e**, Experimental timeline. **f**, Counts of endogenous T cells. **g**, Counts of Foxp3$^+$CD25$^+$CD4$^+$ endogenous Tregs. **h**,**i**, The experimental setting is described in Fig. 1b. CAR-T cells in tumors were classified into several subpopulations based on the gating of CAR density (Fig. 1j). Shown are response curves of MFI of TNFα (**h**) and TIM-3 (**i**) as a function of CAR density (n = 4 mice). Indicated are *P* values. All data represent the mean ± s.e.m. and are analyzed by two-tailed Student's t-test (**a**-**c**, **h**, **i**), or one-way ANOVA with Tukey's multiple-comparisons test (**d**, **f**, **g**). Data are one representative of two independent experiments.

https://doi.org/10.1038/s41587-023-02060-8

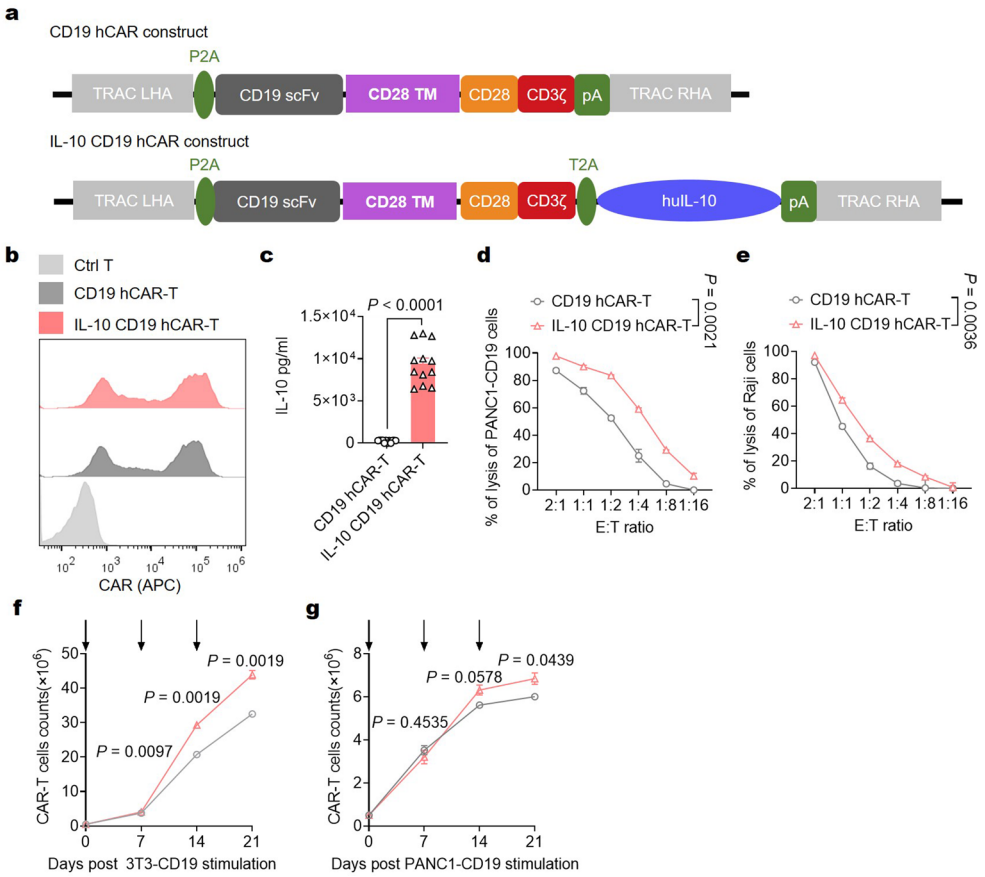

Extended Data Fig. 3 | Preparation and in vitro characterizations of IL-10-secreting CD19 hCAR-T cells. a, Schematic depicting constructs of CD19-targeted second-generation CD28-based human CAR (CD19 hCAR) and human IL-10-secreting CD19 hCAR (IL-10 CD19 hCAR). **b**, The expression levels of CD19 hCAR were analyzed by flow cytometry. Ctrl T, untransduced control human T cells. **c**, The culture supernatants were examined for the concentration of hIL-10 on day 8 after hCAR-T cell preparation (n = 12 biologically independent samples). **d**, **e**, CD19 hCAR-T and IL-10 CD19 hCAR-T cells were cocultured with PANC1-CD19 cells or Raji cells at different E:T ratios for 48 h (n = 3 biologically independent samples). Shown are the percentage of lysis of PANC1-CD19 cell (**d**) or Raji cell (**e**). **f**,**g**, The proliferation of CD19 hCAR and IL-10 CD19 hCAR-T cells after multiple weekly stimulation (indicated by arrows; n = 3) with irradiated NIH/3T3-CD19 (**f**) or PANC1-CD19 (**g**) cells (n = 3 biologically independent samples). All data represent the mean ± s.e.m. and are analyzed by two-tailed Student's t-test. Data are one representative of two independent experiments.

https://doi.org/10.1038/s41587-023-02060-8

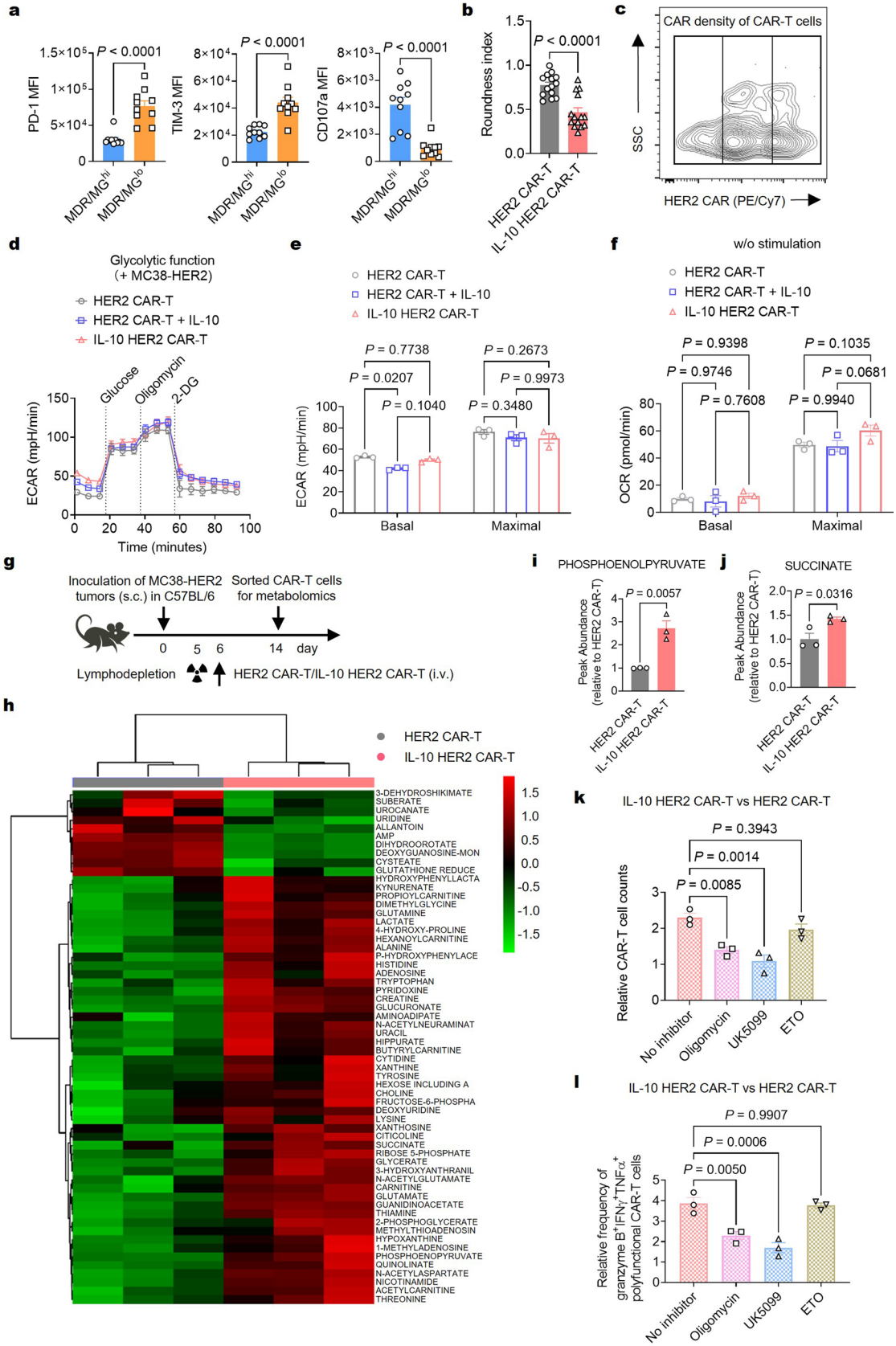

Extended Data Fig. 4 | See next page for caption.

https://doi.org/10.1038/s41587-023-02060-8

Extended Data Fig. 4 | IL-10 expression improved mitochondrial fitness and increased the levels of pyruvate production intermediates and TCA cycle intermediates in CAR-T cells. The experimental setting is described in Fig. 2a. **a**, MFI of PD-1, TIM-3, and CD107a in MDR/MG^{hi} and MDR/MG^{lo} CAR-T cells in tumor (n = 10 mice). **b**, Quantification of roundness index of mitochondria in CAR-T cells as shown in Fig. 2i (n = 15 biologically independent samples). **c**, Representative contour plot showing CAR-T cells in tumor were classified into three subpopulations based on CAR density. **d**-**f**, The experimental setting is described in Fig. 3a-c (n = 3 biologically independent samples). **d**, Real-time analysis of ECAR. **e**, Average basal and maximal ECAR. **f**, Average basal and maximal OCR of HER2 CAR-T and IL-10 HER2 CAR-T cells in the presence or absence of IL-10 without antigen stimulation. **g**-**j**, C57BL/6 mice were inoculated s.c. with MC38-HER2 colon cancer cells (1×10^6), lymphodepleted, and received IL-10 HER2 CAR-T cells or HER2 CAR-T cells (3×10^6, i.v.) on day 6. On day 14, tumor-infiltrating CAR-T cells were sorted for metabolomics analysis (n = 3 biologically independent samples, each sample is pooled from n = 5 mice). **g**, Experimental timeline. **h**, Clustered heatmap of significantly altered metabolites ($P < 0.05$) in HER2 CAR-T and IL-10 HER2 CAR-T cells. The color blocks indicate relative metabolite levels, with high expression in red and low expression in green. **i**,**j**, Fold changes of phosphoenolpyruvate (**i**) and succinate (**j**) (relative to HER2 CAR-T cells). **k**,**l**, HER2 CAR-T or IL-10 HER2 CAR-T cells were cocultured with MC38-HER2 cells in the presence of indicated inhibitors (n = 3 biologically independent samples). Shown are relative CAR-T cell counts (**k**) and relative frequencies of granzyme B$^+$IFNγ$^+$TNFα$^+$ polyfunctional CAR-T cells (**l**) (IL-10 HER2 CAR-T vs. HER2 CAR-T). Data are one representative of two independent experiments. All data represent the mean ± s.e.m. and are analyzed by two-tailed Student's t-test (**a**, **b**, **i**, **j**) or by one- or two-way ANOVA with Tukey's multiple-comparisons test (**e**, **f**, **k**, **l**).

https://doi.org/10.1038/s41587-023-02060-8

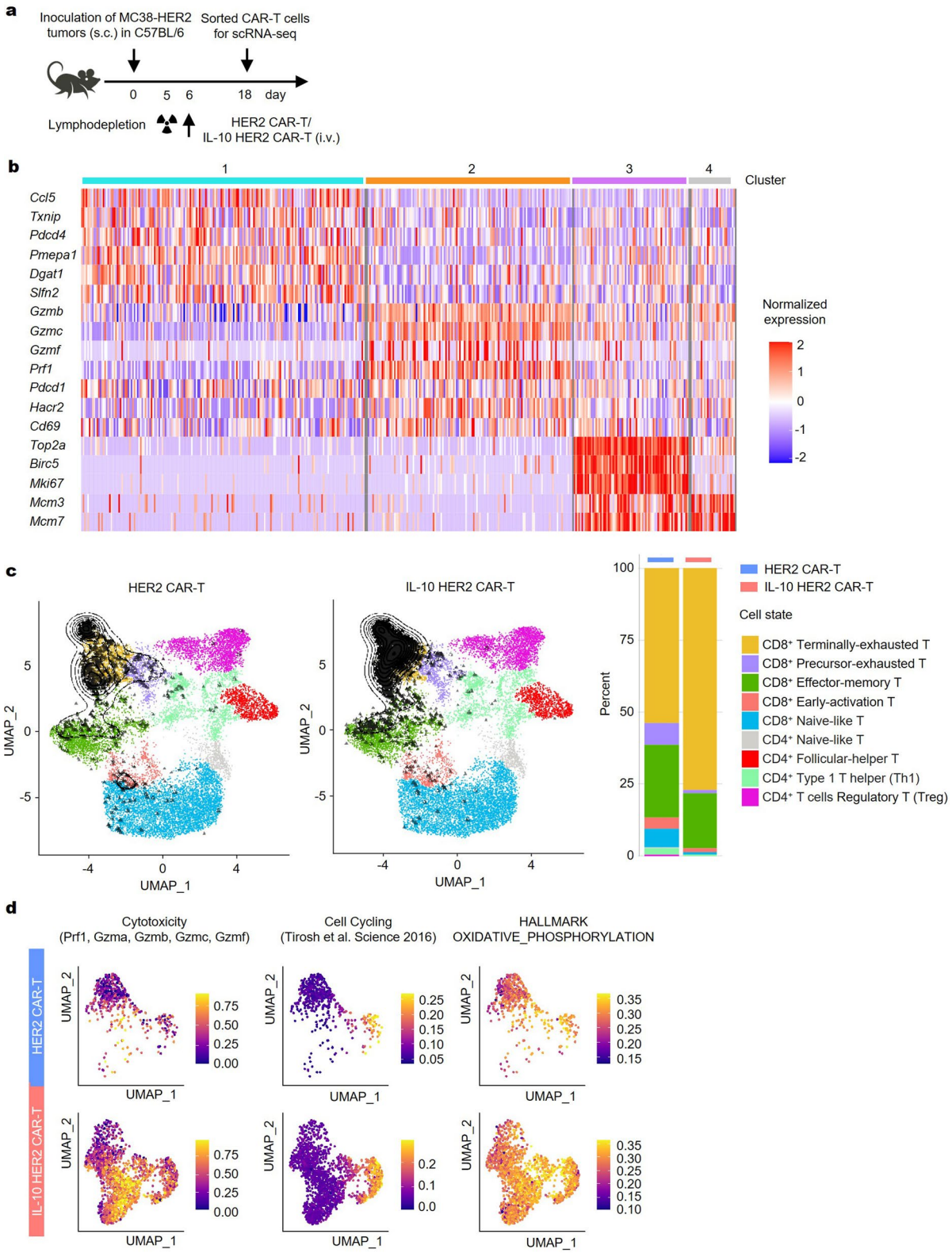

Extended Data Fig. 5 | IL-10-expressing HER2 CAR-T cells exhibit an expanded subpopulation of CD8$^+$ terminally exhausted T cells with upregulated gene expression encoding cell cycling, cytotoxicity, and OXPHOS. a, The experimental setting and timeline is described in Fig. 4. **b**, Heatmap representing the expression levels of representative marker genes in each cluster. **c**, Projection of IL-10 HER2 CAR-T cells and HER2 CAR-T cells into a reference atlas of tumor-infiltrating lymphocytes. Reference atlas states are indicated as colored cells. CD8$^+$ terminally-exhausted T cell cluster was characterized as high expression of granzymes, multiple inhibitory receptors (*Pdcd1, Ctla4, Lag3, Tigit, Havcr2*/TIM-3, etc.) and *Tox*[16]. Shown are cell subtype compositions for each group. Black contour lines represent the density of projected cells. **d**, Gene signature scores for each group of samples (HER2 CAR-T and IL-10 HER2 CAR-T cells) for the indicated gene sets.

https://doi.org/10.1038/s41587-023-02060-8

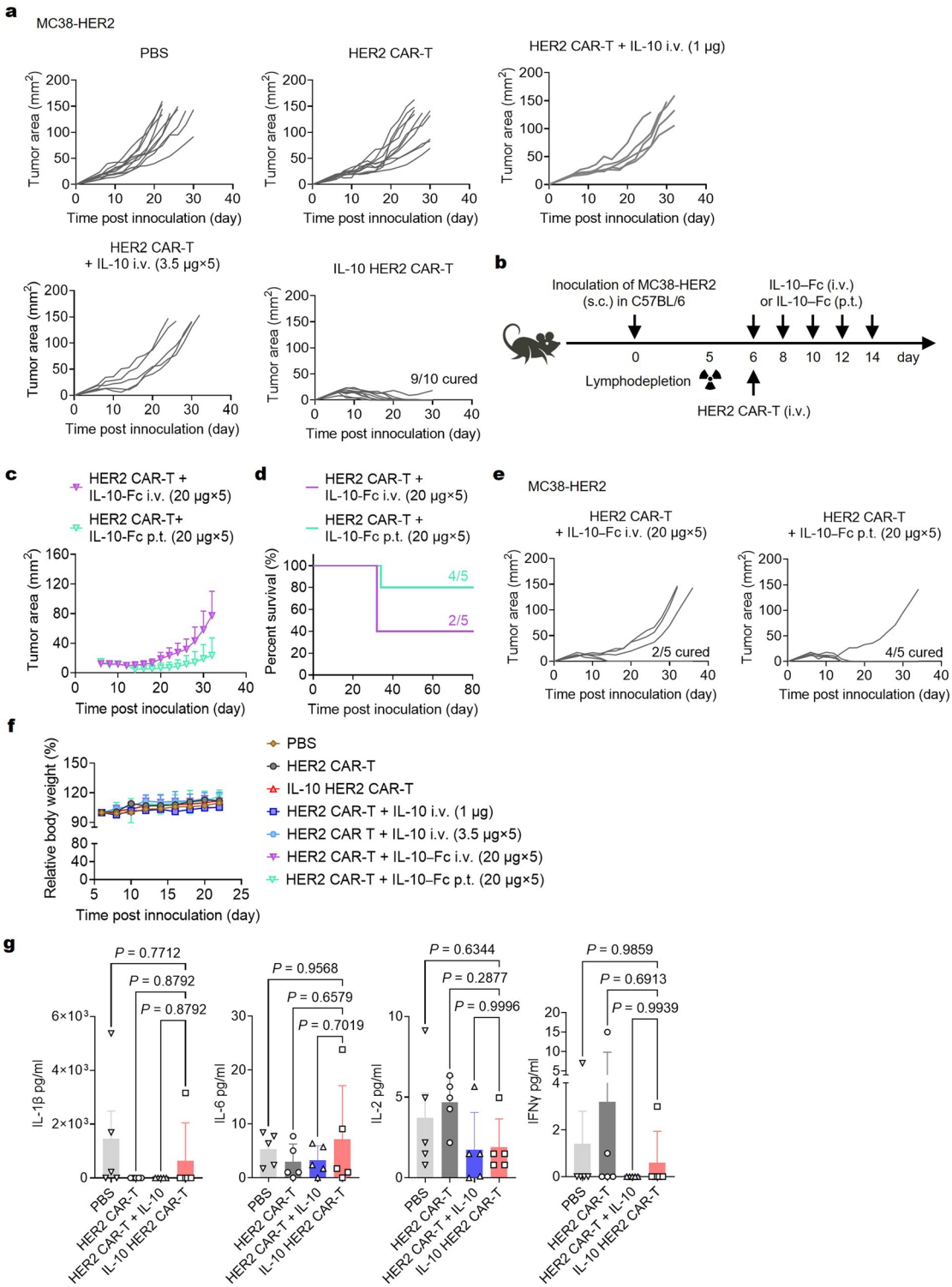

Extended Data Fig. 6 | In vivo assessment of therapeutic efficacy and toxicity of IL-10 HER2 CAR-T cells in the MC38-HER2 tumor model. a, Experimental setting is described in Fig. 5a. Shown are individual tumor growth curves. Indicated are numbers of tumor-free mice among the total number of mice in the group (**a**). **b**-**e**, The experimental setting was the same as described in Fig. 5a except another two treatment groups were added: HER2 CAR-T cells (3×10^6) in combination with IL-10 – Fc[12] (20 μg × 5, equivalent to native IL-10 at the dose of 3.5 μg × 5) through i.v. or peritumoral (p.t.) administration (n = 5 mice). Shown are experimental timeline (**b**), average tumor growth curves (**c**), survival curves (**d**), and individual tumor growth curves (**e**). Indicated are numbers of tumor-free mice among the total number of mice in the group (**d**, **e**). **f**, Body weight of treated mice in both Fig. 5b and Extended Data Fig. 6c (n = 10 mice for the PBS, HER2 CAR-T, and IL-10 HER2 CAR-T groups, and n = 5 mice for the rest of the groups). **g**, The experimental setting was the same as described in Fig. 1b (n = 5 mice). Serum was collected and examined for the concentration of IL-1β, IL-6, IL-2, and IFNγ by ELISA. All data represent the mean ± s.e.m. and are analyzed by one-way ANOVA with Tukey's multiple-comparisons test.

https://doi.org/10.1038/s41587-023-02060-8

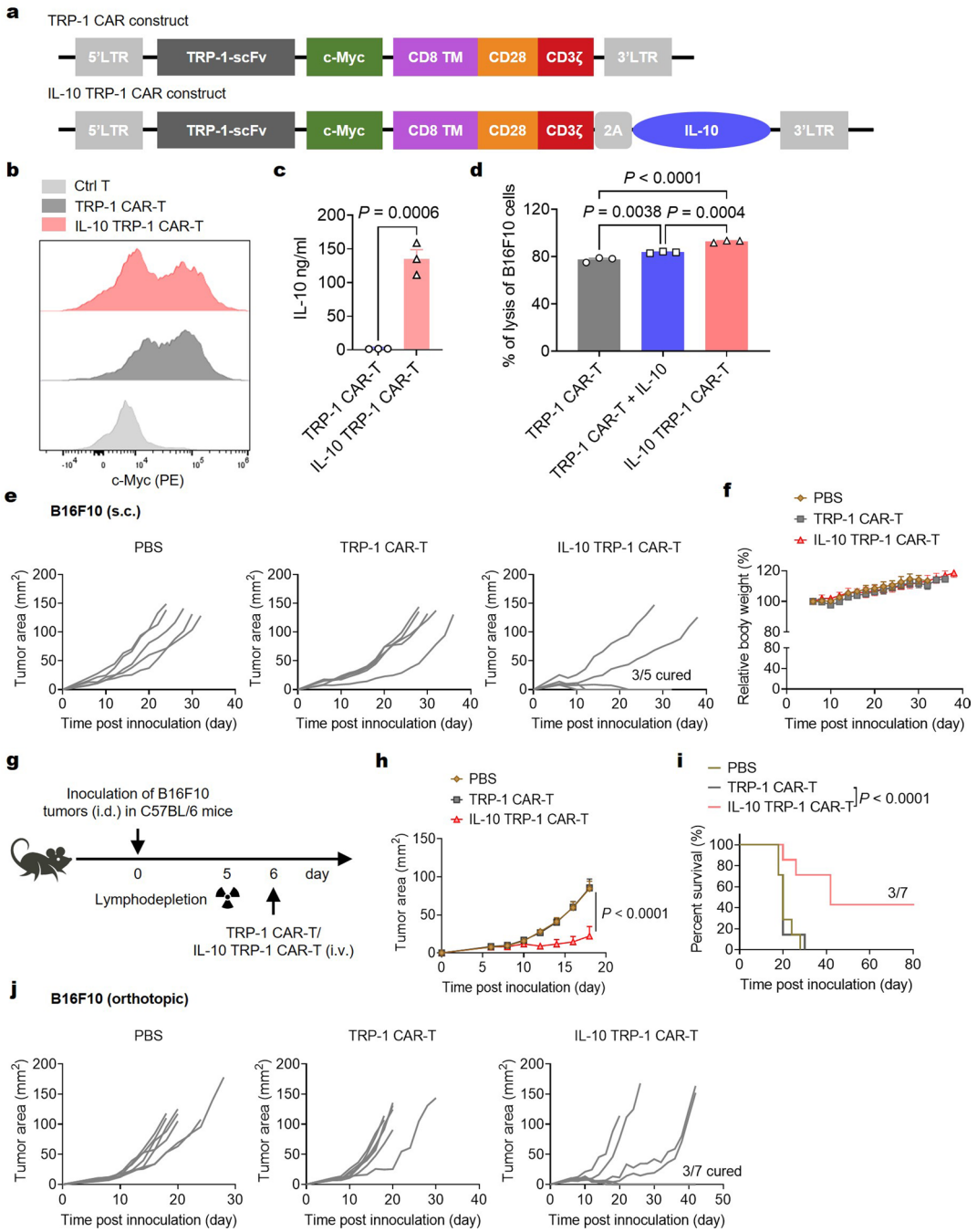

Extended Data Fig. 7 | Preparation and efficacy assessment of TRP-1 CAR-T cells in the subcutaneous and orthotopic B16F10 tumor models. a, Schematic depicting constructs of TRP-1-directed second-generation CD28-based CAR (TRP-1 CAR) and murine IL-10-secreting TRP-1 CAR (IL-10 TRP-1 CAR). **b**, The expression levels of TRP-1 CAR were examined by staining the c-Myc tag. Ctrl T, untransduced T cells as control. **c**, IL-10 TRP-1 CAR-T or TRP-1 CAR-T cells were co-cultured with B16F10 cells for 3 days (n = 3 biologically independent samples). The culture supernatants were examined for the concentration of IL-10 by ELISA. **d**, IL-10 TRP-1 CAR-T or TRP-1 CAR-T cells in the absence or presence of IL-10 (145 ng/ml) were cocultured with B16F10 cells at the E:T ratio of 0.5:1 for 48 h (n = 3 biologically independent samples). The percentage of tumor cell lysis was analyzed by flow cytometry. **e**,**f**, Experimental setting is described in Fig. 5d (n = 5 mice). Shown are individual tumor growth curves (**e**) and relative body weight (**f**). Indicated are numbers of tumor-free mice among the total number of mice in the group (**e**). **g**-**j**, C57BL/6 mice were inoculated intradermally (i.d.) with B16F10 cells (2×10^5) to establish an orthotopic melanoma model. Mice were then lymphodepleted, and received i.v. adoptive transfer of IL-10 TRP-1 CAR-T cells (3×10^6), or TRP-1 CAR-T cells (3×10^6) on day 6 (n = 7 mice). **g**, Experimental timeline. **h**-**j**, Shown are average tumor growth curves (**h**), mouse survival curves (**i**), and individual tumor growth curves (**j**) of the orthotopic B16F10 melanoma model. Indicated are numbers of tumor-free mice among the total number of mice in the group (**i**,**j**). All data represent the mean ± s.e.m. and are analyzed by two-tailed Student's t-test (**c**), or by one- or two-way ANOVA with Tukey's multiple-comparisons test (**d**, **h**), or by log-rank test (**i**).

https://doi.org/10.1038/s41587-023-02060-8

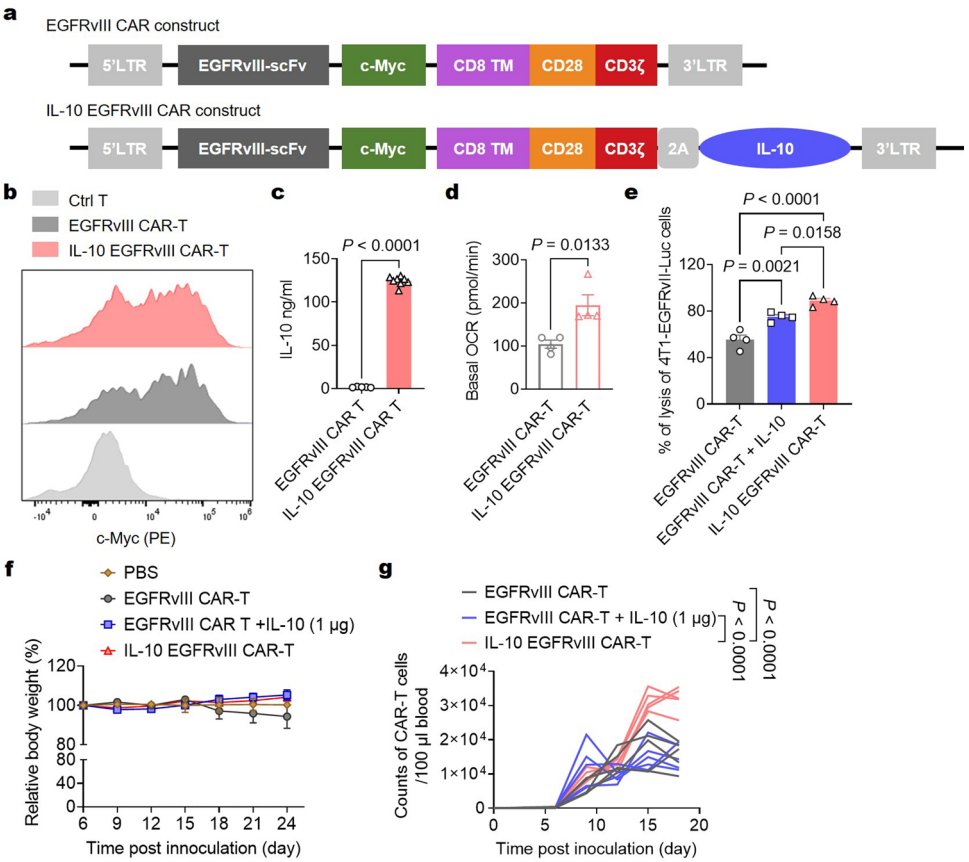

Extended Data Fig. 8 | Preparation and efficacy assessment of EGFRvIII CAR-T cells in the 4T1-EGFRvIII-Luc tumor model. a, Schematic depicting constructs of EGFRvIII-directed second-generation CD28-based CAR (EGFRvIII CAR), and murine IL-10-secreting EGFRvIII CAR (IL-10 EGFRvIII CAR). **b**, The expression levels of EGFRvIII CAR were examined by staining the c-Myc tag. Ctrl T, untransduced T cells as control. **c**, EGFRvIII CAR-T or IL-10 EGFRvIII CAR-T cells were co-cultured with 4T1-EGFRvIIII-Luc cells for 3 days (n = 5 biologically independent samples for EGFRvIII CAR-T, n = 10 biologically independent samples for EGFRvIII CAR-T). The culture supernatants were examined for the concentration of IL-10 by ELISA. **d**, IL-10 EGFRvIII CAR-T or EGFRvIII CAR-T cells in the presence or absence of IL-10 were cocultured with 4T1-EGFRvIII-Luc cells at the E:T ratio of 5:1 for 18 h (n = 4 biologically independent samples). CAR-T cells were then isolated for a seahorse assay. Shown are average basal OCR. **e**, IL-10 EGFRvIII CAR-T or EGFRvIII CAR-T cells in the absence or presence of IL-10 (145 ng/ml) were cocultured with 4T1-EGFRvIIII-Luc cells at the E:T ratio of 0.5:1 for 48 h (n = 4 biologically independent samples). The percentage of tumor cell lysis was analyzed by flow cytometry. **f**, Experimental setting is described in Fig. 5 **f** (n = 5 mice). Shown are relative body weight. **g**, BALB/c mice were i.v. inoculated with 4T1-EGFRvIII-Luc cancer cells (5×10^4), lymphodepleted, and received i.v. adoptive transfer of IL-10 EGFRvIII CAR-T cells (3×10^6), or EGFRvIII CAR-T cells (3×10^6) in the presence or absence of i.v. administered IL-10 (1 μg) on day 6 (n = 5 mice). On day 6, 9, 12, 15, and 18, the blood samples were collected and analyzed by flow cytometry. Shown are counts of viable EGFRvIII CAR-T cells in the peripheral blood of individual mouse. All data represent the mean ± s.e.m. and are analyzed by two-tailed Student's t-test (**c**, **d**), or by one- or two-way ANOVA with Tukey's multiple-comparisons test (**e**, **g**). Data are one representative of two independent experiments.

https://doi.org/10.1038/s41587-023-02060-8

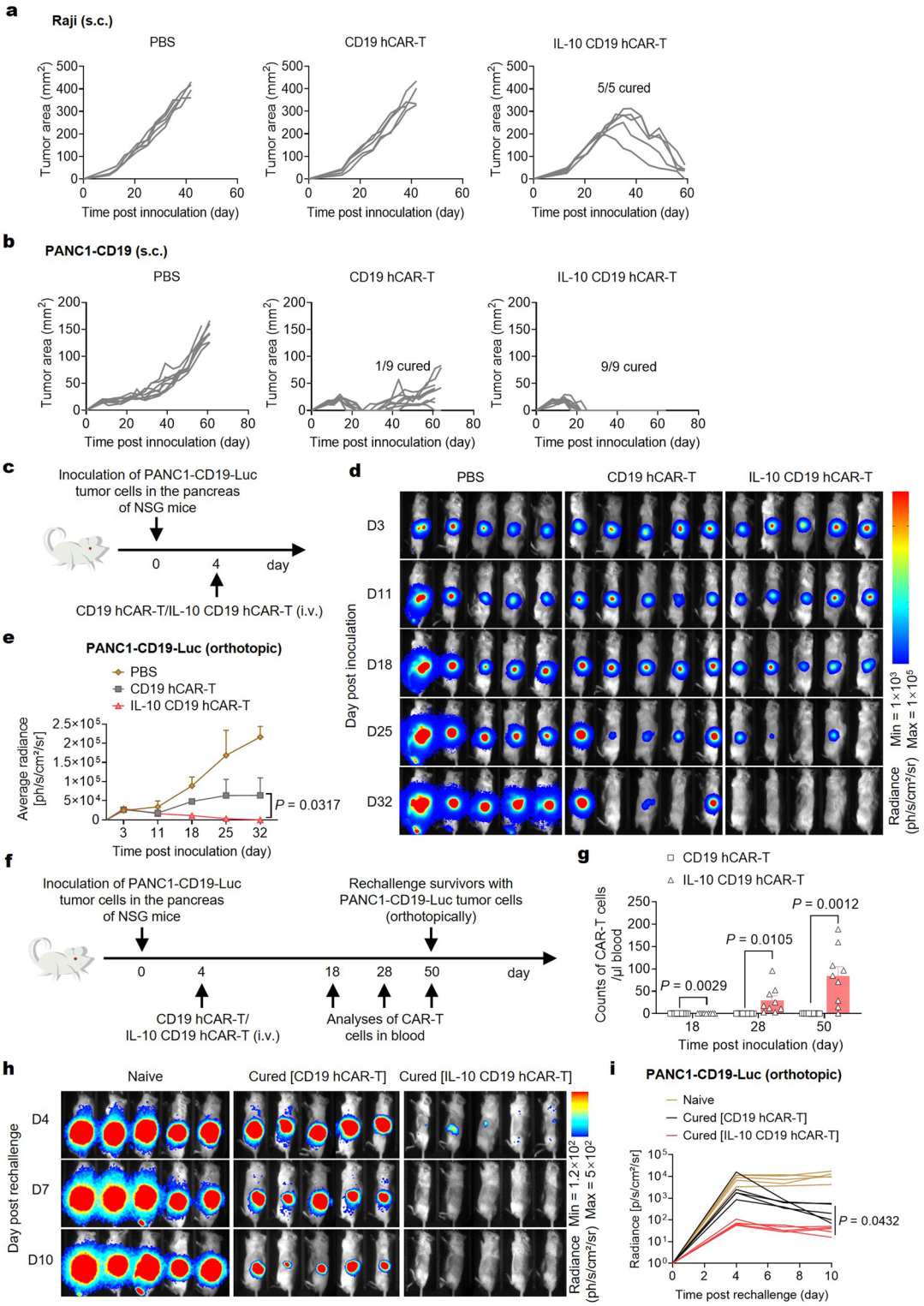

Extended Data Fig. 9 | See next page for caption.

https://doi.org/10.1038/s41587-023-02060-8

Extended Data Fig. 9 | Efficacy assessment of hCAR-T cells in the subcutaneous Raji and PANC1-CD19 xenograft tumor models, and the orthotopic PANC1-CD19-Luc xenograft tumor model. a, **b**, Experimental setting is described in Fig. 5i. **a**, **b**, Shown are individual tumor growth curves of the subcutaneous Raji model (**a**) and PANC1-CD19 model (**b**). Indicated are numbers of tumor-free mice among the total number of mice in the group (**a**, **b**). **c**-**e**, PANC1-CD19-Luc human epithelioid carcinoma cells (2×10^6) were implanted in the tail of the pancreas of NSG mice to establish an orthotopic human PDAC model. Mice were then received i.v. adoptive cell transfer of CD19 hCAR-T or IL-10 CD19 hCAR-T cells (1×10^5) on day 4 (n = 5 mice). **c**, Experimental timeline. **d**, Longitudinal bioluminescent imaging was performed to monitor orthotopic tumor growth. **e**, Average radiance (p/s/cm2/sr) of mice of different treatment groups. **f**-**i**, PANC1-CD19-Luc human epithelioid carcinoma cells (2×10^6) were orthotopically implanted in the tail of the pancreas of NSG mice. Mice were then received i.v. adoptive cell transfer of CD19 hCAR-T or IL-10 CD19 hCAR-T cells (5×10^5) on day 4 (n = 5 mice). On day 18, 28 and 50, the blood samples were collected and analyzed by flow cytometry. Survivors from treatment groups of CD19 hCAR-T and IL-10 CD19 hCAR-T were rechallenged orthotopically with PANC1-CD19-Luc (2×10^6) cells on day 50 post primary inoculation. Naive NSG mice were inoculated with the same number of tumor cells as controls. **f**, Experimental timeline. **g**, Shown are counts of viable hCAR-T cells in peripheral blood on day 18, 28 and 50. n = 10 mice pooled from two independent experiments. **h**, Longitudinal bioluminescent imaging was performed to monitor tumor growth post rechallenge (n = 5 mice). **i**, Individual radiance (p/s/cm2/sr) showing the rechallenged tumor growth of survivors from indicated treatment groups (n = 5 mice). All data represent the mean ± s.e.m. and are analyzed by two-tailed Student's t-test (**g**, **i**), or by Mann–Whitney U test (**e**). Data are one representative of two independent experiments.

https://doi.org/10.1038/s41587-023-02060-8

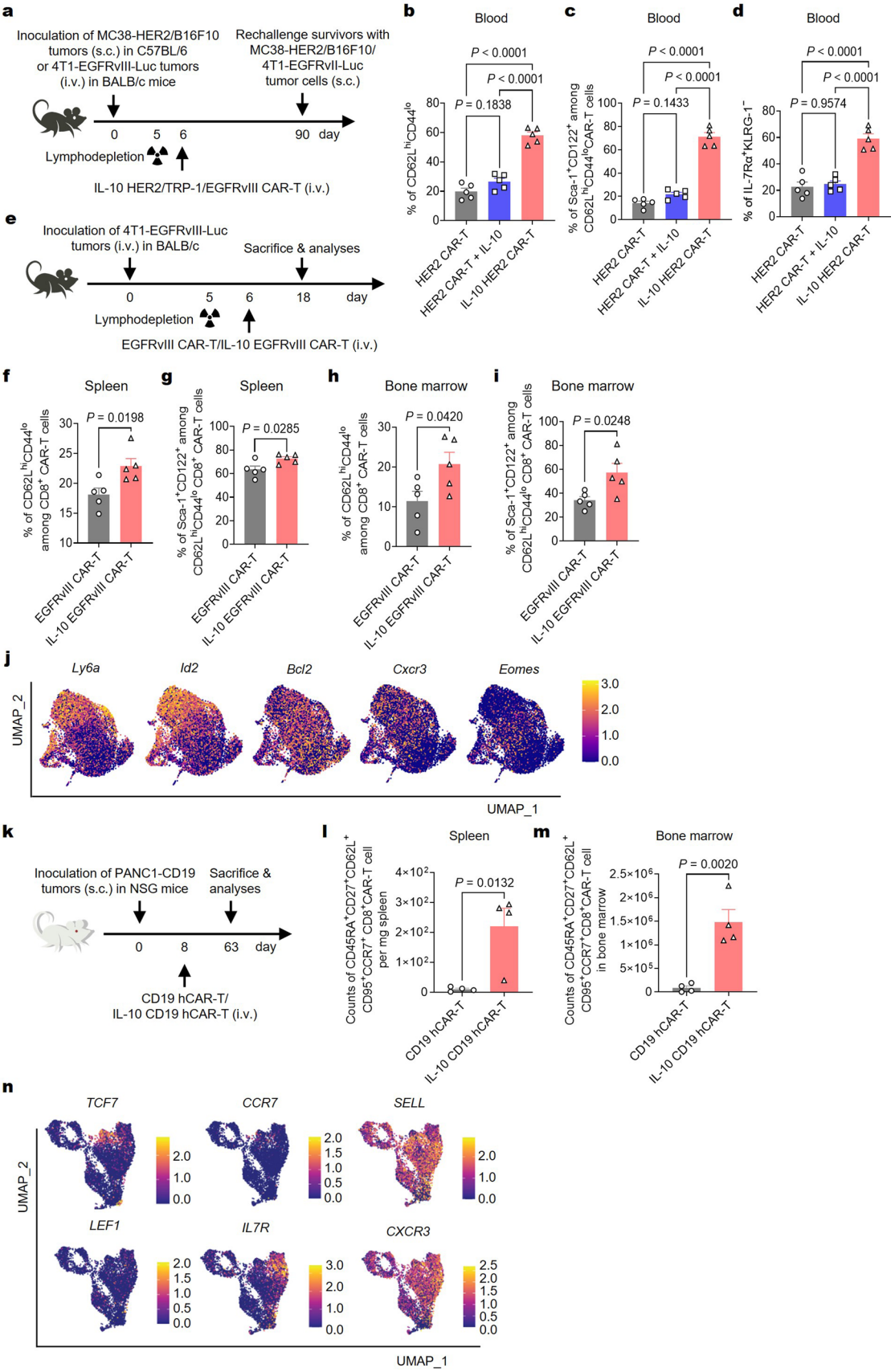

Extended Data Fig. 10 | See next page for caption.

https://doi.org/10.1038/s41587-023-02060-8

Extended Data Fig. 10 | IL-10 expression promotes stemness in mouse and human CAR-T cells. a, The experimental timeline for Fig. 6a-c. **b**-**d**, The experimental setting is described in Fig. 6d (n = 5 mice). Shown are frequencies of $CD62L^{hi}CD44^{lo}$ cells among total CAR-T cells (**b**) and $Sca\text{-}1^{+}CD122^{+}$ cells among $CD62L^{hi}CD44^{lo}$ CAR-T cells (**c**) in blood. **d**, Shown are the frequencies of $IL\text{-}7R\alpha^{+}KLRG\text{-}1^{-}$ among total CAR-T cells in blood. **e**-**i**, BALB/c mice were inoculated with 4T1-EGFRvIII-Luc (5×10^4, i.v.), sublethally lymphodepleted by irradiation on day 5, and received i.v. adoptive transfer of IL-10 EGFRvIII CAR-T cells (3×10^6), or EGFRvIII CAR-T cells (3×10^6) on day 6 (n = 5 mice). On day 18, mice were killed for phenotype analyses of CAR-T cells in spleen and bone marrow by flow cytometry. **e**, Experimental timeline. **f**, **h**, Average frequencies of $CD62L^{hi}CD44^{lo}$ cells among total CAR-T cells in spleen (**f**) and bone marrow (**h**). **g**, **i**, Average frequencies of $Sca\text{-}1^{+}CD122^{+}$ cells among $CD62L^{hi}CD44^{lo}$ CAR-T cells in spleen (**g**) and bone marrow (**i**). **j**, The experimental setting is described in Fig. 6d. Shown are single-cell expression of key marker genes over the UMAP representation of the map. **k**-**m**, NSG mice were inoculated (s.c.) with PANC1-CD19 cells (2×10^6) and received i.v. adoptive cell transfers of CD19 hCAR-T cells (1×10^6) or IL-10 CD19 hCAR-T cells (1×10^6) on day 8 (n = 4 mice). On day 63, mice were killed for phenotype analyses of CAR-T cells in spleen and bone marrow by flow cytometry. **k**, Experimental timeline. **l**, **m**, Shown are counts of $CD45RA^{+}CD27^{+}CD62L^{+}CD95^{+}CCR7^{+}$ human $CD8^{+}$ CAR-T cells in spleen (**l**) and bone marrow (**m**). **n**, The experimental setting is described in Fig. 6k. Shown are single-cell expression of key marker genes over the UMAP representation of the map. All data represent the mean ± s.e.m. and are analyzed by two-tailed Student's t-test (**f**, **g**, **h**, **i**, **l**, **m**), one-way ANOVA with Tukey's multiple-comparisons test (**b**-**d**).

nature portfolio

Corresponding author(s): Li Tang, Yugang Guo, Jie Sun

Last updated by author(s): Oct 9, 2023

Reporting Summary

Nature Portfolio wishes to improve the reproducibility of the work that we publish. This form provides structure for consistency and transparency in reporting. For further information on Nature Portfolio policies, see our Editorial Policies and the Editorial Policy Checklist.

Statistics

For all statistical analyses, confirm that the following items are present in the figure legend, table legend, main text, or Methods section.

n/a	Confirmed
☐	☒ The exact sample size (*n*) for each experimental group/condition, given as a discrete number and unit of measurement
☐	☒ A statement on whether measurements were taken from distinct samples or whether the same sample was measured repeatedly
☐	☒ The statistical test(s) used AND whether they are one- or two-sided *Only common tests should be described solely by name; describe more complex techniques in the Methods section.*
☐	☒ A description of all covariates tested
☐	☒ A description of any assumptions or corrections, such as tests of normality and adjustment for multiple comparisons
☒	☐ A full description of the statistical parameters including central tendency (e.g. means) or other basic estimates (e.g. regression coefficient) AND variation (e.g. standard deviation) or associated estimates of uncertainty (e.g. confidence intervals)
☐	☒ For null hypothesis testing, the test statistic (e.g. *F*, *t*, *r*) with confidence intervals, effect sizes, degrees of freedom and *P* value noted *Give P values as exact values whenever suitable.*
☒	☐ For Bayesian analysis, information on the choice of priors and Markov chain Monte Carlo settings
☒	☐ For hierarchical and complex designs, identification of the appropriate level for tests and full reporting of outcomes
☒	☐ Estimates of effect sizes (e.g. Cohen's *d*, Pearson's *r*), indicating how they were calculated

Our web collection on statistics for biologists contains articles on many of the points above.

Software and code

Policy information about availability of computer code

Data collection	Flow cytometry data collection was performed with Attune NxT Software version 3 (Thermal Fischer Scientific) or LSRFortessa with FACSDiva Software version 8.0.1 (BD Biosciences). Transmission electron microscopy data collection was performed using Velox imaging software (Thermal Fischer Scientific). In vivo bioluminescence data collection was performed using Living Image Software (PerkinElmer). Seahorse data was collected using Seahorse Wave Desktop Software (Agilent). Metabolomics data was collected using the Agilent Quantitative analysis software (version B.07.00, MassHunter Agilent technologies). csRNA sequencing data was collected on a HiSeq4000 (Illumina).

Data analysis	Flow cytometry data were analyzed using FlowJo 10.8.1 (Tree Star, Oregon, USA). Statistical analysis was performed using GraphPad Prism 9 (GraphPad software, Inc, La Jolla, CA, USA). Relative quantification of metabolites was based on EIC (Extracted Ion Chromatogram) areas for the monitored MRM transitions. Signal intensity drift correction and noise filtering was done within the MRM PROBS software. The preprocessed data with peak areas were imported into Metaboanalyst 5.0 for further data analysis. csRNA sequencing raw data of mouse intratumoral HER2 CAR-T cells and human splenic CD19 CAR-T cells were demultiplexed by cellranger mkfastq from 10x Genomics (version 3.0.2) and primary data analysis performed with Cell Ranger (version 2.2.0) using a custom reference package based on mouse reference genome (mm10 or GRCh38) and GENCODE gene models. csRNA sequencing raw data of mouse splenic HER2 CAR-T cells CeleScope rna from Singleron (version 3.0.1) and primary data analysis was performed with CeleScope (version 1.10.0) using a custom reference package based on reference genome (Mus_musculus_ensembl_92). Unsupervised clustering was performed on the PC reduction using the FindNeighbors and FindClusters functions implemented in Seurat with parameters k.param=30 and resolution=0.35. Differentially expressed genes between clusters were determined using the FindMarkers function of Seurat, which applies a Wilcoxon test to determine significance. Differentially expressed genes were visualized using the EnhancedVolcano R package (https://github.com/kevinblighe/EnhancedVolcano) with cutoff on log2(fold-change)=0.5 and p-value=10-5. Gene sets for relevant biological processes and pathways were obtained from the database mSigDB, and signature scores for these gene sets were calculated using the UCell package. Gene set enrichment analysis between clusters was performed on average gene expression by cluster using the R package clusterProfiler and relevant signatures from mSigDB.40 and relevant signatures from mSigDB. Projection of HER2 CAR-T or IL-10 HER2 CAR-T cells into a reference atlas of TILs was performed using the ProjecTILs methodwith default parameters.

For manuscripts utilizing custom algorithms or software that are central to the research but not yet described in published literature, software must be made available to editors and reviewers. We strongly encourage code deposition in a community repository (e.g. GitHub). See the Nature Portfolio guidelines for submitting code & software for further information.

Data

Policy information about availability of data

All manuscripts must include a data availability statement. This statement should provide the following information, where applicable:

- Accession codes, unique identifiers, or web links for publicly available datasets
- A description of any restrictions on data availability
- For clinical datasets or third party data, please ensure that the statement adheres to our policy

All data generated and supporting the findings of this study are available within the paper. The scRNA-seq data for murine CAR-T cells from this study have been deposited in the GEO under accession number 245517. The scRNA-seq data for the human CAR-T cells are available in the CNGB Sequence Archive (CNSA) of China National GeneBank Database with accession number CNP0003547. The R code required to reproduce the scRNA-seq data shown in Fig. 4, Fig. 6, Extended Data Fig. 5 Extended Data Fig.10 is alailable at the following repository: http://github.com/carmonalab/LiTang_IL10_CART. The reference genme for primary data analysis of HER2 CAR-T cells in tumors was mm10, GRCh38 for CD19 hCAR-T cells, and ensembl_92 for HER2 CAR-T cells in spleen. Source Data are provided with the online version of the paper. Additional information and materials will be made available upon reasonable request.

Field-specific reporting

Please select the one below that is the best fit for your research. If you are not sure, read the appropriate sections before making your selection.

☒ Life sciences ☐ Behavioural & social sciences ☐ Ecological, evolutionary & environmental sciences

For a reference copy of the document with all sections, see nature.com/documents/nr-reporting-summary-flat.pdf

Life sciences study design

All studies must disclose on these points even when the disclosure is negative.

Sample size	Group sizes for in vivo validation experiments were selected empirically based on previous results of the intragroup variation of tumor growth upon similar treatments. Similarly, group sizes in vitro were selected on the basis of prior knowledge of variation. Ref: Nat Immunol 2021 Jun; 22(6):746.756
Data exclusions	Rout outlier tests were run with default parameters (Q = 1%) in Prism on all mouse experimental data due to inherent variability within the model system.
Replication	All presented results were repeatable. Replicates were used in all experiments as noted in figure legend or methods.
Randomization	Age and sex-matched animals were used for each experiment. Mice were randomized prior to treatment. In the in vitro experiments, samples with same pretreatment conditions were randomly assigned to a treatment group with a pipette.
Blinding	No blinding was performed due to requirements for cage labeling and staffing needs.

Reporting for specific materials, systems and methods

We require information from authors about some types of materials, experimental systems and methods used in many studies. Here, indicate whether each material, system or method listed is relevant to your study. If you are not sure if a list item applies to your research, read the appropriate section before selecting a response.

Materials & experimental systems

n/a	Involved in the study
☐	☒ Antibodies
☐	☒ Eukaryotic cell lines
☒	☐ Palaeontology and archaeology
☐	☒ Animals and other organisms
☐	☒ Human research participants
☒	☐ Clinical data
☒	☐ Dual use research of concern

Methods

n/a	Involved in the study
☒	☐ ChIP-seq
☐	☒ Flow cytometry
☒	☐ MRI-based neuroimaging

Antibodies

Antibodies used

The following antibodies or staining reagents were purchased from BioLegend: CD16/32 (93, 101302), CD45.2 (104, 109814), CD8β (YTS256.7.7, 126606), CD4 (RM4-5, 100526), NK1.1 (PK136, 108740), F4/80 (BM8,123108), CD3ε (17A2, 100306), CD11c (N418, 117348), I-A/I-E (MHC-II, M5/114.15.2, 107643), Siglec-F (S17007L, 155508), CD80 (16-10A1, 104734), CD86 (GL-1, 105006), CD11b (M1/70, 101228), Ki67 (16A8, 652424), Granzyme B (GB11, 515403), IFNγ (XMG1.2, 505826), TNFα (MP6-XT22, 506308), IL-2 (JES6-5H4, 503822), Gr-1 (RB6-8C5, 202519), PD-1 (29F.1A12, 135216), TIM-3 (RMT3-23, 119706). CD107a (H4A3, 328608), CD44 (IM7, 103028), CD62L (MEL-14, 104432), CD122 (5H4, 105906), Sca-1 (D7, 108106), KLRG1 (2F1/KLRG1, 138410), IL-7Rα (SB/199, 121111), human CD95 (DX2, 305606), Streptavidin-PE/Cyanine7 (405206), human Granzyme B (QA16A02, 372208), human IFN-γ (B2, 552887). The following antibodies or staining reagents were purchased from BD Biosciences: human CD4 (SK3, 563550), human CD8 (SK1, 557834). The following antibodies or staining reagents were purchased from Invitrogen: human CD62L(DREG56, 48-0629-42), human CD45RA (H100, 69-0458-42), human CD27 (O323, 56-0279-42), CCR7 (3D12, 61-1979-42). Biotinylated Human Her2/ErbB2 Protein (HE2-H822R) was purchased from ACROBiosystems. Myc-tag antibody (9B11, 3739) was obtained from Cell Signaling Technology. Goat anti-mouse IgG was purchased from Jackson ImmunoResearch (Polyclonal, 115-606-003), In VivoMAb anti-mouse CD3 (BE0002, 17A2) and In VivoMab anti-mouse CD28 (BE0015-1, 37.51) were purchased from BioXcell.

Validation

Validated by manufacturer as indicated on the websites. In Vivo anti-mouse CD3 and CD28 were used for stimulate the proliferation and cytokine production of murine T cells. The other antibodies described above are applied to Flowcytometry in this study, and thier validation can be found on the manufacturer website. Antibodies with human reactivity are labeled as such, remaining antibodies without labels have mouse reactivity.

Eukaryotic cell lines

Policy information about cell lines

Cell line source(s)

HER2 transduced MC38 mouse colon cancer cells (MC38-HER2) were provided by Prof. Pedro Romero (University of Lausanne). B16F10 melanoma cells, Phoenix-Eco cell sand Raji cells were originally obtained from the American Type Culture Collection. 4T1-EGFRvIII-Luc mouse breast cancer cells were provided by Prof. Darrell J. Irvine (Massachusetts Institute of Technology). NIH/3T3-CD19 cells, PANC1-CD19 cells and PANC1-CD19-Luc cells were generated by Prof. Jie Sun (Zhejiang University).

Authentication

None of the cell lines were authenticated in these studies. In all related studies, cell lines with low passage number were used.

Mycoplasma contamination

All cell lines were confirmed mycoplasma negative.

Commonly misidentified lines
(See ICLAC register)

No commonly misidentified cell lines were used.

Animals and other organisms

Policy information about studies involving animals; ARRIVE guidelines recommended for reporting animal research

Laboratory animals

Five to six-week old female C57BL/6 (C57BL/6J) mice, BALB/c (BALB/cByJ) mice were purchased from Charles River Laboratories (Lyon, France). Six to twelve-week old NOD/SCID/IL-2Rγ null mice were purchased from GemPharmatech (Nanjing, China). T-cell receptor (TCR)-transgenic OT-I mice (C57BL/6-Tg(TcraTcrb)1100Mjb/J) were originally purchased from The Jackson Laboratory (Bar Harbor, ME, USA) and maintained in École Polytechnique Fédérale de Lausanne (EPFL)-Center of PhenoGenomics (CPG) animal facility. Mpc1fl/fl mice were crossed to Cd4cre mice on an OT-I background to generate MPC1 knock out (MPC1-KO) OT-I mice. Mpc1 fl/fl breeder mice and OT-I breeder mice range in age from six to 40 weeks. Six to twelve-week OT-I T mice and MPC1-KO OT-I mice were used for T cell isolation. Mice were housed under a controlled 12-hour light and 12-hour dark cycle, with tempratures maintained between 22-24 degree and humidity levels between 40-60% to ensure a comfortable environment.

Wild animals

Study did not involve wild animals.

Field-collected samples

Study did not involve field-collected samples.

Ethics oversight

Experimental procedures in syngeneic mouse studies were approved by the Swiss authorities (Canton of Vaud, animal protocol ID 3206 and 3533) and NSG mouse studies were approved by Institutional Animal Care and Use Committee of Zhejiang University

(Hangzhou, China, animal protocol NO.2021914). Animal studies were performed in accordance with the guidelines from CPG of EPFL, the animal facility of University of Lausanne, and Zhejiang University. Mice were euthanized when body weight loss was beyond 15% of baseline weight, tumor area reached 150 mm2 (syngeneic mouse models) or the maximum diameter reached 20 mm (NSG mouse models), or any signs of discomfort were detected by the investigators or as recommended by the veterinarian who monitored the mice every other day.

Note that full information on the approval of the study protocol must also be provided in the manuscript.

Human research participants

Policy information about studies involving human research participants

Population characteristics	Whole blood samples from healthy volunteers (female/male, 19-32 years old) were collected by a doctor of the First Affiliated Hospital of Zhejiang University School of Medicine
Recruitment	Volunteers recruitment occurred through campus public media. Healthy volunteers aged 18-35 with written informed consent were recruited and the protocol was approved by the Ethics Committee of Zhejiang University School of Medicine (Hangzhou, China, NO.2020-067). Donors were compensated according to Institute policy of Zhejiang University School of Medicine. Other than ensuring good health, no other bias were identifed. While variability among different donors may affect batch-to batch variability, it impact on comparing treatment groups within the same batch of T cells is minor.
Ethics oversight	Ethics Committee of Zhejiang University School of Medicine (Hangzhou, China, NO.2020-067).

Note that full information on the approval of the study protocol must also be provided in the manuscript.

Flow Cytometry

Plots

Confirm that:

☒ The axis labels state the marker and fluorochrome used (e.g. CD4-FITC).

☒ The axis scales are clearly visible. Include numbers along axes only for bottom left plot of group (a 'group' is an analysis of identical markers).

☒ All plots are contour plots with outliers or pseudocolor plots.

☒ A numerical value for number of cells or percentage (with statistics) is provided.

Methodology

Sample preparation	Tumors were dissected from the surrounding tissues, weighed, mechanically minced, and stirred at 1000 rpm in RPMI-1640 medium with Collagenase Type IV (1 mg/mL, Gibco / Thermo Fisher Scientific), Dispase II (100 µg/mL, Sigma-Aldrich, St. Louis, Missouri, USA), Hyalurondase (100 µg/mL, Sigma-Aldrich), and DNase I (100 µg/mL, Sigma-Aldrich) at 37 °C for 60 min for digestion. Red blood cell lysis was performed on the tumor digestion samples with ACK Lysing Buffer (Gibco / Thermo Fisher Scientific), and then tumor-infiltrating leukocytes were then enriched by density gradient centrifugation against Percoll (GE healthcare) and resuspended in PBS with bovine serum albumin (0.2%, wt/v, Sigma-Aldrich). Spleen were dissected from the surrounding tissues, grinned, and filtered with strainers. Red blood cell lysis was performed on the spleen samples with ACK Lysing Buffer and then resuspended in PBS with bovine serum albumin (0.2%, wt/v, Sigma-Aldrich). Blood samples were collected from abdominal aorta, and resuspend in PBS with 2mM EDTA. Red blood cell was removed by ACK lysis buffer(Gibco / Thermo Fisher Scientific), then red blood cell debris were removed by density gradient centrifugation against Percoll (GE healthcare), and then resuspended in PBS with bovine serum albumin (0.2%, wt/v, Sigma-Aldrich). Bone marrow was harvested from freshly isolated femurs and tibiae. Bones were crushed in 5 ml of PBS with ethylenediaminetetraacetic acid (2mM, Sigma-Aldrich) and filtered with strainers. Remaining RBCs were lysed with ACK buffer.
Instrument	Data were collected using Attune NxT Flow Cytometer (Invitrogen / Thermal Fischer Scientific) or LSRFortessa Flow Cytometer (BD Biosciences). Cell sorting was performed with FACS Aria II (BD Biosciences).
Software	Flow cytometry data were analyzed using FlowJo 10.8.1 (Tree Star, Oregon, USA). Flow cytometry data collection was performed using Attune NxT Software version 3 (Invitrogen / Thermal Fischer Scientific) or LSRFortessa with FACSDiva Software (BD Biosciences).
Cell population abundance	Purity was determined by flow cytometry for CAR positive T cells (> 95 %).
Gating strategy	We used standard gating strategies: gating on the typical lymphocyte population based on FSC-SSC signals, doublet exclusion based on FSC-H and FSC-A comparison, Live/Dead discrimination based on DAPI or fixable Aqua dye signals. Cell populations were identified based on the expression markers listed below. CAR-T cells: CD45+/CD3+/CAR+; natural killer cells: CD45+/CD3-/NK1.1+; dendritic cells: CD45+/Gr-1-/CD11b+/CD11c+/MHCII+; Tumor-associated macrophages: CD45+/Gr-1-/CD11b+/F4/80+/MHCII+; Gr-1+CD11b+ Myeloid-Derived Suppressor Cells: CD45+/Gr-1+/CD11b+; Eosinophils: CD45+/CD11b+/Siglec-F+. All the representative FACS gating strategies were described in Supplemental Fig. 1.

☒ Tick this box to confirm that a figure exemplifying the gating strategy is provided in the Supplementary Information.